

Review

Deactivation Mechanism and Anti-Deactivation Measures of Metal Catalyst in the Dry Reforming of Methane: A Review

Bo Yuan ^{1,†}, Tao Zhu ^{1,2,*}, Yiwei Han ¹, Xueli Zhang ¹, Meidan Wang ¹ and Chen Li ¹

¹ School of Chemical & Environmental Engineering, China University of Mining & Technology (Beijing), Beijing 100083, China

² Shaanxi Key Laboratory of Lacustrine Shale Gas Accumulation and Exploitation (under Planning), Research Institute of Yanchang Petroleum (Group) Co., Ltd., Xi'an 710065, China

* Correspondence: bamboozt@cumtb.edu.cn; Tel.: +86-010-62339170

† These authors contributed to the work equally and should be regarded as co-first authors.

Abstract: In recent decades, the massive emission of greenhouse gases, such as carbon dioxide and methane, into the atmosphere has had a serious impact on the ecological environment. The dry reforming of carbon dioxide and methane to syngas cannot only realize the resource utilization of methane and carbon dioxide but also reduce global climate change. It is of great significance in carbon emission reduction. Owing to the dry reforming of methane (DRM) being a strongly endothermic reaction, it needs to be carried out under high-temperature conditions. It makes the catalyst have problems of the sintering of metal, carbon deposition, and poisoning. This article revolves around the problem of catalyst deactivation during the DRM reaction. It expands upon the thermodynamics and mechanisms of the DRM reaction, analyzes the causes of metal catalyst deactivation due to carbon deposition, sintering, and poisoning, and summarizes how the active components, supports, and additives of metal catalysts restrain the DRM catalyst deactivation during the reaction. The analysis revealed that changing the type and size of the active metal, adjusting the properties of the support, and adding additives can further regulate the dispersion of the active component, the interaction between the active component and the support, the oxygen vacancies of the support, and the acidity and basicity of the catalyst surface, ultimately achieving control over the metal catalyst's resistance to sintering, carbon deposition, and sulfur poisoning. In addition, it discusses the application of metal catalysts in photothermal and plasma-catalyzed DRM. Finally, it outlines the prospects for research on metal catalysts for the DRM.

Keywords: carbon emission reduction; dry reforming of methane; metal catalyst; sintering; carbon deposition



Citation: Yuan, B.; Zhu, T.; Han, Y.; Zhang, X.; Wang, M.; Li, C. Deactivation Mechanism and Anti-Deactivation Measures of Metal Catalyst in the Dry Reforming of Methane: A Review. *Atmosphere* **2023**, *14*, 770. <https://doi.org/10.3390/atmos14050770>

Academic Editors: Viney Aneja and Kumar Vikrant

Received: 5 March 2023

Revised: 28 March 2023

Accepted: 21 April 2023

Published: 23 April 2023



Copyright: © 2023 by the authors. Licensee MDPI, Basel, Switzerland. This article is an open access article distributed under the terms and conditions of the Creative Commons Attribution (CC BY) license (<https://creativecommons.org/licenses/by/4.0/>).

1. Introduction

A shortage of energy and environmental pollution are two key issues in the sustainable development of humans. With the increase in the world population and the rapid development in industry, the demand for energy continues to increase each year. Society's dependence on fossil fuels contributes to massive emissions of greenhouse gases; of particular concern is carbon dioxide (CO₂), which has exacerbated global climate change and has had a serious impact on the ecological environment [1]. Methane (CH₄), a trace component of the global atmosphere, is much less concentrated than CO₂ and is more active in the atmosphere than CO₂. Additionally, the greenhouse effect of CH₄ is 23–28 times that of CO₂, which is a “super greenhouse gas” with a rapid warming effect [2]. Carbon peaking and carbon neutrality are important initiatives to mitigate global climate change; therefore, it is of great significance currently to abate CH₄ and CO₂. In order to reduce the emission of these two major greenhouse gases, technological methods such as capture, catalytic conversion, and storage have been adopted, in which the conversion of CH₄ and CO₂

into high-value-added products or liquid fuels by means of catalytic conversion has high economic value [3–5].

The dry reforming of methane (DRM) is a popular research topic because it has the advantage of simultaneously eliminating CH_4 and CO_2 and converting these two greenhouse gases into hydrogen (H_2) and carbon monoxide (CO), which have shown excellent performance in clean energy [6]. DRM is the dry reforming reaction of CO_2 and CH_4 as feedstock to produce industrially valuable syngas ($n(\text{H}_2):n(\text{CO}) = 1:1$) [7]. This method can achieve the direct conversion of two major greenhouse gases, making it a green and sustainable pathway. Additionally, the syngas can be used for the synthesis of oxygen-containing compounds as well as high-carbon hydrocarbon fuels, which have good application prospects [8]. DRM has the following advantages: 1. The simultaneous utilization and elimination of two greenhouse gases CO_2 and CH_4 , effectively mitigating environmental problems such as global warming and major climate change [9]. 2. The synthesis gas generated by this reaction has a molar ratio of H_2/CO which is close to 1, which is ideal for the Fischer–Tropsch synthesis of oxygenated compounds and long-chain hydrocarbons and is conducive to industrial applications. 3. It provides a pathway for the direct utilization of biogas [10]. However, CH_4 and CO_2 have stable chemical structures, and how to catalyze CH_4 and CO_2 in a directional manner for direct conversion to high-value-added syngas is one of the important challenges for C1 catalysis science today [11,12]. In the DRM reaction, the catalyst plays a critical role in the production of syngas. It can maximize the production of syngas, help to change and increase the reaction rate, and can significantly reduce the temperature required for the reaction [13].

For the DRM reaction, many transition metals such as Ir, Rh, Pd, Pt, Ru, Ni, and Co have been investigated as active components of catalysts to accelerate this reaction. Noble metals as active components can display excellent catalytic activity and stability, especially in terms of resistance to carbon deactivation. It has been reported that the noble metal activity order is $\text{Rh} > \text{Ru} > \text{Ir} > \text{Pt} > \text{Pd}$ [14]. Non-noble metal Ni- and Co-based catalysts have good low-temperature catalytic activity but are easily deactivated by carbon deposition and sintering, limiting their application in the DRM reactions [15]. Noble metal catalysts are generally considered to be less susceptible to sulfur poisoning than non-noble metal catalysts [16]. In order to overcome the deactivation caused by metal catalyst sintering, carbon deposition, and sulfur poisoning, researchers have investigated various factors to reduce or eliminate their effects, including changing the type and size of active metals, changing supports, adding additives, changing preparation methods, etc., and have then regulated the dispersion of the metal active component, the interaction between the active component and the support, and the oxygen vacancies on the surface of the support as well as the acidity and basicity of the catalyst surface, and have finally realized the anti-sintering ability, anti-carbon deposition ability, and anti-sulfur ability of the metal catalyst regulation.

Extensive research has been conducted on the deactivation of metal-based catalysts in the dry reforming of methane (DRM) reaction, with efforts focused on finding solutions to this issue. In the past few years, several academic review papers have been published on this topic, each with a different focus. General overviews of DRM catalyst design and development can be found in the papers by Kawi et al. [17], Abdulrasheed et al. [18], and Aramouni et al. [19]. Bian et al. [20] reviewed and discussed Ni-based bimetallic catalysts for the DRM, emphasizing the synergistic effects that address catalyst deactivation. Sharif-anjazi et al. [21] provided an overview of the theoretical viewpoints on preventing coking in the DRM using Ni- and Co-based nanocatalysts. Baharudin et al. [22] provided a discussion on the impact of operating parameters on the DRM reaction in their review of DRM catalyst design, as well as how to manipulate them to manage/control the formation of coke during the DRM process. Pakhare et al. [23] provided a comprehensive review of the progress in developing high-activity, high-stability, noble metal-based DRM catalysts. Photothermal and plasma-catalyzed DRM reactions have also received widespread attention and research.

However, there is currently a lack of discussion on the mechanism of sulfur poisoning in the DRM reaction.

In recent years, the comprehensive utilization of greenhouse gases CH₄ and CO₂ has attracted widespread attention, many different types of DRM catalysts have emerged, and the research on related reaction mechanisms has gradually deepened. In order to understand the research status of DRM metal catalysts, the article first summarizes the thermodynamics and reaction mechanism of the DRM reaction. Next, it analyzes the main reasons for the deactivation of metal catalysts in the DRM reaction. Then, the recent research progress on the restraint of deactivation of the DRM reaction catalysts is elaborated upon from the perspectives of the active components, supports, and additives that affect the performance of catalysts. Finally, the application of metal catalysts in photothermal and plasma catalysis for the DRM is discussed.

2. Thermodynamics and Reaction Mechanism of DRM Reaction

2.1. Thermodynamics of DRM Reaction

A thermodynamic investigation of the DRM reaction can determine the optimal reaction temperature, reaction pressure, and gas feed ratio to obtain low-cost and high-yield syngas. DRM is a strong heat-absorbing reversible reaction that requires high temperatures to convert CH₄ and CO₂ into CO and H₂ syngas, and the use of catalysts can significantly reduce the reaction temperature and increase the reaction rate, as well as prevent other detrimental secondary reactions from occurring. The DRM reaction is a complex process, with the main reactions being shown in Table 1 [13,24].

Table 1. Main reactions that occur during the DRM process.

| No. | Reaction | Reaction Equation | $\Delta H_{298K}^0 / \text{kJ} \cdot \text{mol}^{-1}$ | Reaction Temperature/°C |
|-----|---|---|---|-------------------------|
| (1) | Main reaction | $\text{CH}_4 + \text{CO}_2 \rightarrow 2\text{CO} + 2\text{H}_2$ | 248 | >640 |
| (2) | Reverse water gas shift reaction | $\text{CO}_2 + \text{H}_2 \rightarrow \text{CO} + \text{H}_2\text{O}$ | 41 | <820 |
| (3) | Methane cracking reaction | $\text{CH}_4 \rightarrow \text{C} + 2\text{H}_2$ | 75 | >527 |
| (4) | Carbon monoxide disproportionation reaction | $2\text{CO} \rightarrow \text{C} + \text{CO}_2$ | −172 | 550~700 |

From the Gibbs enthalpy change in the main reaction (1), it is clear that DRM is a typical strong heat-absorbing reaction that can only occur at thermodynamic temperatures greater than 640 °C. CH₄ and CO₂ are highly stable molecules with high dissociation energies: 435 (CH₃-H) and 526 (CO-O) kJ·mol^{−1}. Therefore, a high temperature is required to achieve the equilibrium conversion of syngas, and catalysts used for the DRM reactions should have strong thermal stability. The main reaction is a volume-increasing reaction, which is beneficial in the positive direction under low pressure; so, the beneficial conditions for the equilibrium to move in the direction of syngas production are high temperature and low pressure. The equilibrium of syngas conversion is usually influenced by the reverse water gas shift (RWGS) reaction (Equation (2)), which occurs at 527–820 °C as shown via thermodynamic calculations. The conditions under which the RWGS reaction does not occur are at lower temperatures and when the CH₄/CO₂ volume ratio is greater than 1. However, when the reaction temperature exceeds 700 °C and the CH₄/CO₂ volume ratio is less than 1, the inverse water gas reaction is violent, which leads to a higher CO₂ conversion rate than the CH₄ conversion rate at equilibrium and favors the production of syngas with an H₂/CO ratio of 1 or less. In addition, the high pressure also favors the positive occurrence of the RWGS reaction.

In addition to the RWGS reaction affecting the reaction, the generation of carbon deposition is often not conducive to the reaction, because it covers the active sites of the catalyst and causes catalyst deactivation. Carbon deposition in the DRM process is mainly attributed to two reactions: the methane cracking reaction (Equation (3)) and the carbon

monoxide disproportionation reaction (Equation (4)). In the carbon monoxide disproportionation reaction, carbon deposition is especially obvious between 550 and 700 °C, while above 900 °C carbon deposition is due to the methane cracking reaction [25,26]. The volume ratio of CH₄/CO₂ in the feed gas, the reaction pressure, and the reaction temperature all affect these reactions and thus the carbon deposition in the catalyst. Several researchers have performed thermodynamic simulations of various temperatures, CO₂/CH₄ ratios, pressures, catalysts, and various carbon deposition reactions, and they have concluded that DRM reactions operating under high temperatures above 850 °C and low pressures are the conditions needed for achieving high conversion rates. Shah et al. [27] used HSC Chemistry thermodynamic software to simulate the product distribution and carbon formation characteristics of the DRM reaction at pressures of 100 kPa and temperatures between 100 °C and 1100 °C. Under the condition of CH₄/CO₂ = 1:1, the yields of H₂ and CO increased with the increase in temperature in this temperature range, in addition to the decrease in H₂/CO and the decrease in carbon deposition. At a temperature of 900 °C and a CH₄/CO₂ molar ratio of 1:1, the values of H₂/CO and H₂O/CO₂ decreased with increasing pressure, indicating that high temperature and low pressure promoted the reaction. Palmer et al. [28] used an online FactSage thermodynamic database to perform thermodynamic calculations of the DRM reactions, in order to determine the equilibrium compositions at different temperatures and the CH₄:CO₂ feed ratios. The results showed that the reaction was favorable at 1000 °C, with excess methane (CH₄:CO₂ = 2:1), atmospheric pressure, complete conversion of CH₄ and CO₂, and no water in the product, suppressing the reverse water gas shift reaction. Moreover, as the CH₄/CO₂ feed ratio increased from 0 to 2, the ratio of H₂ to CO also increased to above 1:1, but the C species content also increased. They solved the problem of carbon deposition by efficiently converting CH₄ and CO₂ into syngas and separable stoichiometric solid carbon using a molten metal alloy catalyst in a bubble column reactor. Li et al. [29] investigated the effect of reaction temperature on the activity of a Ni/MoCeZr/MgAl₂O₄-MgO catalyst at a CO₂/CH₄ volume ratio of 1:1. The results showed that the activity and stability of Ni/MoCeZr/MgAl₂O₄-MgO increased with an increase in reaction temperature, and at 1000 °C the conversion of both of the maximum values of CH₄ and CO₂ occurred. As for the amount of carbon deposition, the amount of carbon deposition on the surface of Ni/MoCeZr/MgAl₂O₄-MgO gradually increased with an increase in the proportion of CH₄ in the feed gas, while the amount of carbon deposition decreased when the proportion of CO₂ increased, and the high reaction temperature was favorable to reduce the formation of carbon deposition.

In conclusion, for the DRM reactions, minimizing the amount of carbon deposition on the catalyst is particularly important for the stable operation of the DRM process [30]. The optimal reaction conditions for the DRM optimized according to thermodynamics are as follows: temperatures of 850~900 °C and low pressure, which are favorable in order to reduce the amount of carbon deposition and promote the reaction. In addition, by adjusting the CH₄/CO₂ feed ratio, temperature, and residence time, the ratio of H₂/CO products can be easily controlled to obtain the desired proportion of syngas feedstock.

2.2. Reaction Mechanism of DRM

The DRM is a complex reaction process with multiple reaction pathways, and studying its reaction mechanism is beneficial for understanding the cause of carbon deposition and guiding the design and synthesis of catalysts. However, the generation of reaction intermediates in the DRM varies under different catalyst systems and reaction conditions, leading to differences in the reaction mechanism. The elementary reaction mechanism of the DRM is usually divided into three steps: CH₄ dissociation, CO₂ dissociation, and intermediate product oxidation. For CH₄ dissociation, four-step sequential dehydrogenation occurs as follows: Step 1: CH₄*+*→CH₃*+H*; Step 2: CH₃*+*→CH₂*+H*; Step 3: CH₂*+*→CH*+H*; Step 4: CH*+*→C*+H*. The adsorption and dissociation of CH₄ on the catalyst surface is the key step in the rate control of the DRM reaction, and the rate of CH₄ dissociation accelerates with an increase in temperature, as shown by a number of

investigations [30]. There are currently three possible reaction paths for CO₂ dissociation: Pathway 1: CO₂*+*→CO*+O*; Pathway 2: CO₂*+H*→COOH*+*→CO*+OH*; Pathway 3: CO₂*+H*→HCOO*+*→CHO*+O*; CHO*→CO*+OH*. For CO₂ dissociation, Pathway 1 describes the direct dissociation of CO₂ adsorbed by the catalyst into CO and O, and the CO₂ reaction induced by catalyst-adsorbed H may be the reason for the formation of Pathways 2 and 3. In addition, the intermediate product CH_X (X = 0–3) generated by the dissociation of CH₄ can be oxidized by the adsorbed O and OH. For example, CH can be oxidized by O(CH*+O*→CHO*+*→CO*+H*) and OH(CH*+OH*→CHOH*+*→CHO*+H*), or it can be dissociated directly to C and H. Free C can be oxidized by O(C*+O*→CO*) and OH(C*+OH*→COH*) as well. Gaining a deep understanding of the detailed surface DRM reaction mechanism of a catalyst is quite challenging; thus, experimental and density functional theory (DFT) calculations need to be combined to speculate on the reaction pathways on the atomic scale, analyze the DRM catalytic reaction mechanism, and elucidate the migration and transformation paths of reactants and intermediate products on the catalyst active sites.

Wang et al. [31] compared the DRM reaction mechanism of NiCe_{0.1}/HAP and Ni/HAP catalysts with the assumed catalyst model and mechanism shown in Figure 1a,b, which is consistent with the elementary reaction mechanism of the above three steps. CH₄ undergoes adsorption and dissociation on metal Ni to form CH_X, CO₂ undergoes adsorption and dissociation on metal Ni or the Ni support interface or support, and the surface oxygen species oxidizes CH_X to form CH_XO, which in turn generates CO and H₂, and finally the desorption of CO and H₂. CH₄ is easily cleaved to inert C atoms on the metal Ni particles, and then C reacts with reactive oxygen to form CO. If the rate of C generation and elimination can be balanced, the activity and stability of the nickel catalyst can be effectively improved. By comparing the reaction mechanism of NiCe_{0.1}/HAP and Ni/HAP catalysts, it was found that the CeO₂-modified Ni particles could partially avoid the further cleavage of C-H of CH₃ into C atoms, thus restraining carbon production. Sagar et al. [32] proposed two pathways for the Ni/MnO_x-CeO₂-catalyzed DRM reaction, as shown in Figure 1c. In Pathway 1, methane cracking is the first and fastest step catalyzed by Ni sites, resulting in CH_X and H_X. Once methane is cracked, CO₂ is adsorbed on the catalyst surface. The H_X produced during methane cracking is used to form bicarbonate, while CH_X further decomposes into C and H₂(g) or H_X on the catalyst surface. The bicarbonate formed then reacts with H_X to release CO and H₂O, and the carbon on the active site is oxidized. In Pathway 2, methane reacts directly with oxygen to generate a carbonyl-type intermediate. The adsorbed carbonyl intermediate reacts with H_X to decompose into CH_X and OH, or the carbonyl can desorb to form CO, while H_X can be combined and desorbed as H₂. CH_X continues to decompose into C and H₂ or H_X, and the resulting carbon is oxidized through Pathway 1 again. Ramon et al. [33] synthesized mixed oxides of La₂Ce₂O₇ and LaNiO₃ with 5% Ni content using the modified Pechini method and hydrothermal method. It was investigated that the pathway reaction of the CH_X* species to produce CH_XO* on La₂Ce₂O₇ and LaNiO₃ mixed oxides synthesized by the two different methods differed, with the formation pathways observed for the catalysts synthesized via the hydrothermal method being CH_X*+OH*↔CH_XO* and CH_X*+O*↔CH_XO*, and the catalysts synthesized via the modified Pechini method only being observed as CH_X*+O*↔CH_XO*, indicating that different synthesis methods synthesize catalysts with different properties, leading to a different reaction mechanism. Wang et al. [34] speculated upon the reaction mechanism of the DRM over the Ni₃ZnCo_{0.7}/Al₂O₃ catalyst by means of in situ FTIR (as shown in Figure 1d), i.e., CH₄ and CO₂ are adsorbed and activated within the Ni₃ZnCo_{0.7}/Al₂O₃ core-shell, CH₄ dissociates to form a carbonate and the CH₃ and H species, and CH₃ further dissociates to the C species, while the H species binds to form desorbed H₂, and the C species is oxidized to form CO via CO₂ being adsorbed into the core-shell. No adsorbed CO peaks were observed on the FTIR spectra; therefore, the pathway of CO₂ dissociation to CO was excluded. During DRM, the bound C atoms in Ni₃ZnCo_{0.7} are consumed via CO₂ oxidation and replenished via CH₄ dissociation, which facilitates the

electron transfer between Ni and Zn atoms and C atoms (as in Figure 1e). Yang et al. [35] described the mechanism of the Ru@SiO₂-catalyzed DRM reaction and elucidated the cause of carbon deposition. First, CH₄ molecules are adsorbed onto the metal Ru and then activated (Equation (5)). Secondly, the adsorbed CH₄ dissociates into H and C atoms (Equation (6)), the adsorbed H atoms combine to form H₂ (Equation (7)), and most of the adsorbed C atoms react with CO₂ to form CO (Equation (8)). The main cause of carbon deposition occurs when the adsorbed carbon atoms combine with each other (Equation (9)). The competition between Equations (8) and (9) determines the extent of carbon deposition, and the activation of CO₂ plays a key role in restraining carbon deposition. The specific reaction mechanism equations are shown in Equations (5)–(9).

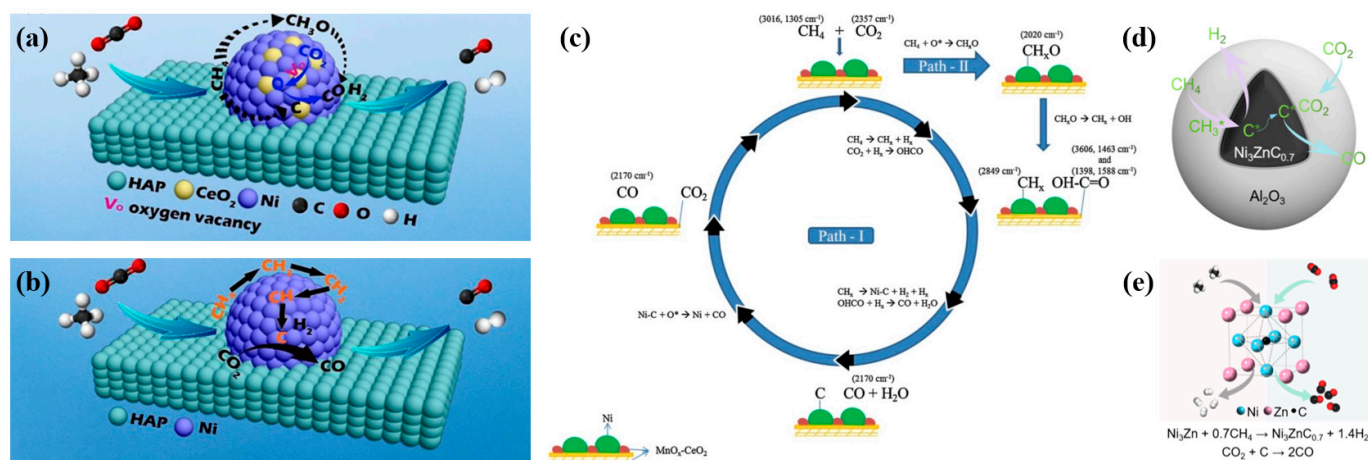
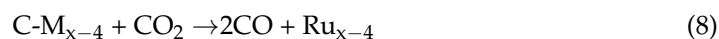
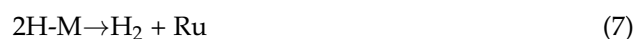
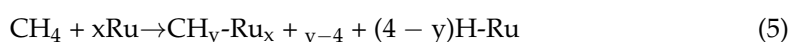


Figure 1. Reaction mechanism of DRM on different catalysts. Possible reaction pathways of methane dry reforming on the (a) NiCe_{0.1}/HAP and (b) Ni/HAP catalysts. (c) Two reaction pathways for the Ni/MnO_x-CeO₂-catalyzed DRM reaction. Schematic illustrations of (d) reaction pathway and (e) carbon storage and release on Ni₃ZnC_{0.7} in the DRM [31,32,34].

In conclusion, the reaction mechanism pathway followed by DRM may be related to the microenvironment of the catalyst surface. The reaction mechanism not only provides insights into the migration and transformation paths of reactants and intermediate products on the catalyst active sites, but also allows for the analysis of the atomic-level reasons for carbon deposition and a development in the effective means and methods to suppress carbon deposition on the catalyst.

3. Deactivation of Metal Catalyst

In the DRM reaction, the challenge is to design a catalyst that remains stable and is less prone to deactivation. Different active metals, supports, promoters, and other factors were tested in the experiments, but it was difficult to obtain the most ideal anti-deactivation

catalyst. All metal catalysts are susceptible to carbon deposition, sintering, and poisoning [36]; thus, researchers are continuously exploring ways to prevent catalyst deactivation caused by carbon deposition, sintering, and poisoning through various approaches such as synthesis methods, catalyst morphology, and mechanism studies.

3.1. Generation of Carbon Deposition in the Reaction Process

DRM was first studied by Fischer and Tropsch in 1923 involving Ni and Co catalysts. They observed severe deactivation due to carbon deposition [37]. As the DRM reaction proceeds, carbon will gradually be deposited on the catalyst. Carbon deposition is mainly attributed to two reactions: the methane cracking reaction (Equation (3)) and the carbon monoxide disproportionation reaction (Equation (4)). In general, when the temperature is 527~627 °C, the two reactions will proceed simultaneously and the carbon deposition effect will be more obvious, while at higher temperatures, CH₄ cracking will be the main carbon deposition reaction and the carbon monoxide disproportionation reaction will generally proceed in the reverse direction, thus eliminating the carbon deposition [17]. The type of carbon deposition can be determined based on the gasification temperature. It is generally believed that there are three types of carbon species: amorphous carbon C_α (300~450 °C), filamentous carbon C_β (450~550 °C), and graphite carbon C_γ (>600 °C) [38]. The mechanism of carbon formation, deposition, and transformation on metal-based catalysts is shown in Figure 2. CO dissociates in contact with the active metal component to produce adsorbed carbon atoms, and C_α reacts with its repeating units to form polymerization into C_β. Under high temperatures, the more reactive C_α and C_β are transformed into the less reactive C_γ.

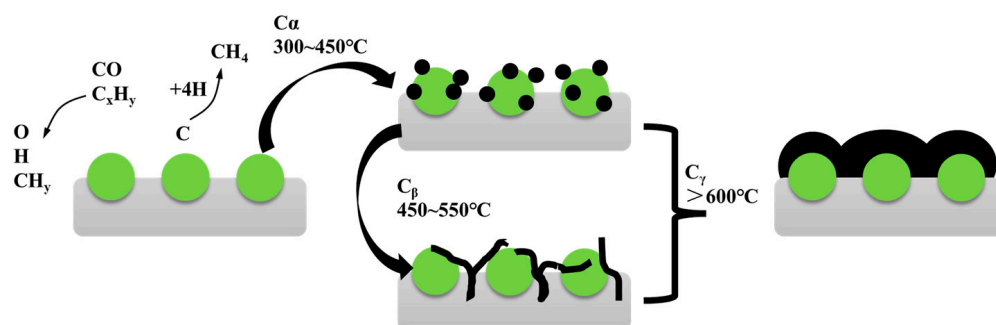


Figure 2. Carbon formation, deposition, and transformation pathways on the metal-based catalyst.

Wang et al. [39] investigated the stability of Ni/CeO₂-com, Ni/CeO₂-HT, and Ni/Ce_{0.9}Eu_{0.1}O_{1.95}-HT catalysts at CH₄/CO₂/N₂ = 1:1:2, 873 K, for 12 h. Compared with the fresh catalysts, carbon deposits were observed in the TEM images of all catalysts in Figure 3a–c, with amorphous carbon formed on the Ni/Ce_{0.9}Eu_{0.1}O_{1.95} surface and filamentous carbon formed on the Ni/CeO₂-com and Ni/CeO₂-HT surfaces. The mechanisms of the deposition and deactivation of carbon using a 20% Ni/Al₂O₃ catalyst in the DRM was investigated by Wang et al. [40] under the DRM reaction conditions of 700 °C and 1 atm; after 30 min, the main type of carbon present was filamentary carbon (as shown in Figure 3d,e), which accounted for about 50% of the catalyst surface. Additionally, graphitic carbon, which could cover and completely deactivate the catalyst, accumulated significantly only in the CO₂-deficient environment. They also found that the carbon deposits on the Ni-based catalyst surface were reaction intermediates generated during the DRM reaction and could be eliminated by the reaction with CO₂. Wang et al. [41] studied the deactivation mechanisms of Ni(111), Ni(211), Ni₃C(001), and Ni₃C(111) crystal planes during the DRM process using first-principle calculations. It was found that the formation of carbon deposits depends on the degree to which CH oxidation dominates the overall reaction and the energy barrier for CO dissociation. The Ni(111) crystal face has a strong ability to resist carbon deposition, while with the Ni(211) and Ni₃C(111) crystal faces it

is easy to deposit carbon on the surface. The characteristics of the easy oxidation of CH bonds and the high dissociation energy barrier of CO bonds are the main reasons for the resistance to carbon deposition on the Ni(111) surface. Predicting the likelihood of carbon deposition from purely theoretical calculations can be tricky since the surface phenomena occurring on the nickel crystals cause substantial deviations from the well-known graphitic carbon thermodynamics [19]. Donphai et al. [42] observed that lower H/C and O/C feed ratios were more prone to carbon deposition in the DRM, and carbon deposition was most likely to occur at feed ratios of 2 for H/C and 1 for O/C. Wang et al. [43] found that the CH_4/CO_2 ratio affects the type of carbon deposition. After synthesizing NiCeAl catalysts using a one-pot method, they found that two types of carbon were formed, namely amorphous carbon and graphitic carbon, where graphitic carbon mainly led to catalyst deactivation. In addition to the feed ratio, the choice of catalyst type, reactor parameters, reaction temperature, support morphology, and the type of additives used also affect the formation of carbon in the DRM process [44].

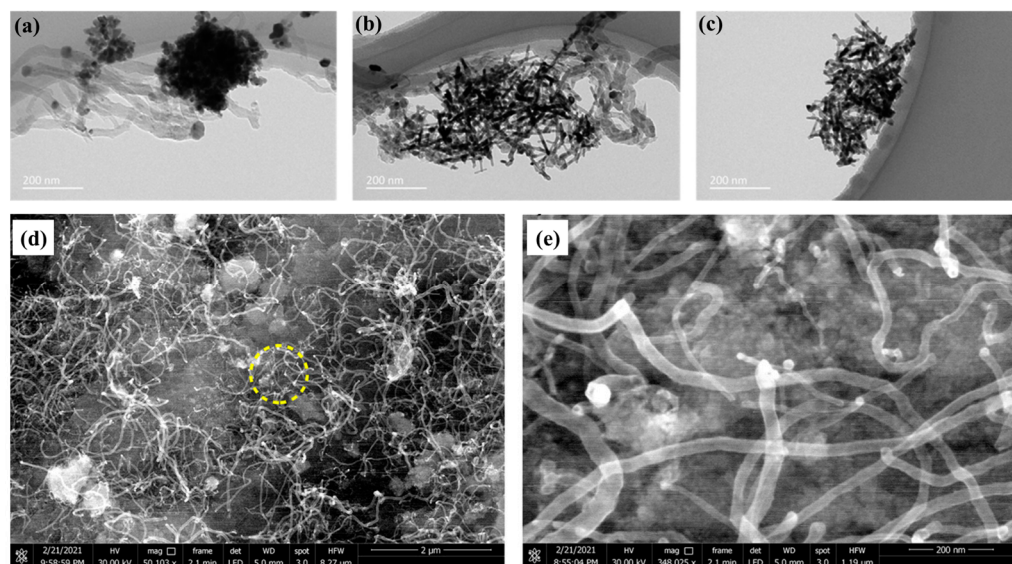


Figure 3. The morphology of different catalyst carbon deposits. TEM images of spent (a) Ni/CeO₂-com, (b) Ni/CeO₂-HT, and (c) Ni/Ce_{0.9}Eu_{0.1}O_{1.95}-HT. SEM images of spent (d,e) 20% Ni/Al₂O₃ [39,40].

During the DRM reaction, carbon deposition mainly leads to catalyst deactivation through three mechanisms: 1. direct adsorption or encapsulation of carbon species onto active metal sites, rendering them inactive; 2. chemical adsorption of carbon species in monolayers or physical adsorption in multilayers on the catalyst surface, thereby blocking the contact of reactant molecules with active metal sites; and 3. the continuous accumulation of filamentous carbon C_β in the catalyst pores, hindering the access of reactant molecules to the active centers, affecting the diffusion of reactants and products, and eventually causing carrier material fracture due to excessive stress, leading to catalyst particle abrasion and bed blockage [18,45].

3.2. Sintering of Active Components in the Reaction Process

The sintering of DMR catalysts is a thermally induced process. During this process, the sintering of active metals can reduce the number of active sites, increase the size of metal particles, block the catalyst's pores, and lower its activity, thereby affecting the diffusion of reactants and products and making carbon deposition more likely to occur. It may also cause some damage to the catalyst bed [46]. Metal sintering is formed in the presence of water in the RWGS reaction and at a temperature of over 700 °C [47]. Sintering usually has two mechanisms: 1. the movement of metal particles in the aggregated state, where the whole metal particles move on the surface of the support through collisions and thus aggregation, and 2. the atomic movement is caused by particle coarsening and Oswald ripening, in which the metal atoms released from the microcrystals move on the surface of the support and are then captured by larger microcrystals. It has been demonstrated that both mechanisms occur simultaneously in the DRM reaction, a process that usually proceeds at a slow rate but is irreversible once the sintering process starts [48,49]. Barrett et al. [50] investigated the structural and electronic changes occurring in the DRM reaction of Co-TiO₂ catalysts by using XRD and XPS and found that the unstable Co phase and sintering led to the formation of large Co microcrystals with an average grain size of 137 nm, resulting in catalyst deactivation, demonstrating that the sintering of the active metal component in the DRM reaction is one of the deactivation mechanisms. Zhang et al. [51] found that Ni/BN-c was rapidly deactivated at 700 °C DRM. They calculated the grain size of fresh and spent Ni/BN-c catalysts based on XRD spectra using Scherrer's equation and found that the grain size of Ni of the spent Ni/BN-c catalyst was 46.3 nm, which was 13.8 nm higher than that of a fresh catalyst (32.5 nm), which led to the rapid deactivation of Ni/BN-c catalysts due to the severe sintering of Ni particles. The interaction strength between the metal and the support has different degrees of influence on the sintering. Chatla et al. [52] prepared a series of Ni/MgO catalysts with different Zr loads via the initial wet impregnation method and applied them to DRM reactions at 500–800 °C. No formation of graphitic carbon was observed in the Ni/1Zr/MgO and Ni/3Zr/MgO catalysts with low Zr loads, suggesting that low Zr loads promote the dispersion of Ni particles and give the catalysts a strong metal–support interaction. Graphitic carbon was found on the Ni/5Zr/MgO and Ni/10Zr/MgO catalysts with high loads of Zr, and the particle size increased after the DRM reaction, indicating that the Ni particles were sintered during the DRM process due to a weak metal–support interaction. Due to the harsh reaction conditions of high temperature and high pressure, it is easy for the DRM reaction to lead to the aggregation and sintering of catalysts. Therefore, the high-heat-stability catalyst can be designed via the limited domain effect strategy to reduce the aggregation and sintering of particles, so as to improve the anti-sintering performance of the catalyst. Liu et al. [53] synthesized 15% Ni/S-1 catalysts using the dissolution–recrystallization method and the impregnation method, respectively. After catalyst performance tests, it was found that the Ni particles on the 15% Ni/S-1 catalyst synthesized via the dissolution–recrystallization method were still well dispersed (as in Figure 4a), but the average size increased to about 8 nm, which may be due to the slight fragmentation of the zeolite. In contrast, the 15% Ni/S-1 catalyst synthesized via the impregnation method was sintered severely, and the average size of the Ni particles increased dramatically to about 26 nm within 8 h (as in Figure 4b). The sintering of Ni particles reduces the active sites of the catalyst, thus decreasing the catalytic activity and stability of the catalyst. This difference proves that Ni nanoparticles confined in the matrix of the S-1 molecular sieve have better anti-sintering properties and thus better catalytic stability. Han et al. [54] designed and developed a Ni-based catalyst on a SiO₂ support with very high resistance to sintering in the DRM reaction. The analysis revealed that the catalyst has a core–shell structure, which enables the catalyst to maintain the Ni nanoparticle state at higher temperatures.

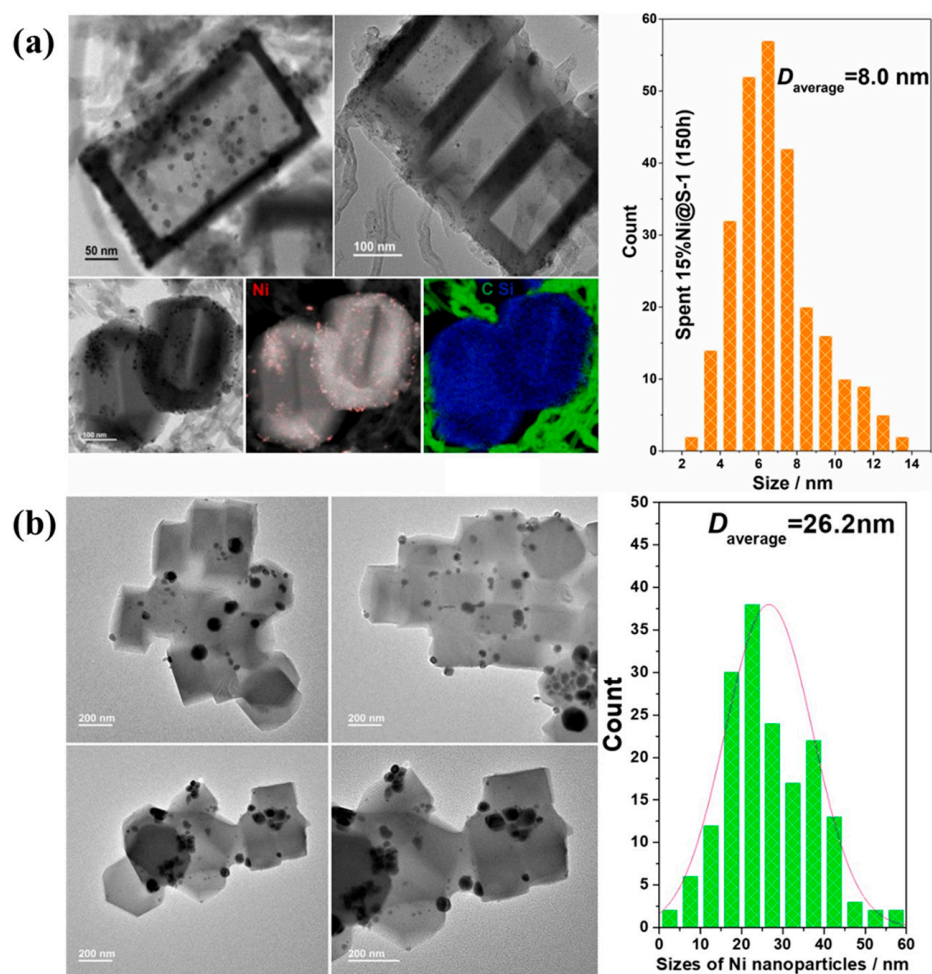


Figure 4. Characterizations of the spent catalysts: (a) 15% Ni/S-1 catalyst via dissolution-recrystallization; (b) 15% Ni/S-1 catalyst via impregnation [53].

3.3. Sulfur Poisoning

In addition to carbon deposition and sintering, another technical challenge in DMR is the impact of sulfur-containing compounds on catalyst activity. Natural gas and biogas are the two most important sources of methane, but both contain sulfur compounds (especially H_2S). It has been shown that the presence of very low concentrations of H_2S can significantly affect catalyst activity and cause sulfur poisoning [11]. Audasso et al. [55] found that the CH_4 conversion of the SYTRh5 catalyst was significantly reduced and severely deactivated by the passage of H_2S gas in the ongoing DRM reaction. The performance of phosphorus-modified rhodium-based catalysts against sulfur poisoning in DMR reactions was investigated by Cimino et al. [56]. In transient and steady-state sulfur poisoning experiments during DMR, it was shown that the sulfur species directly attack and bind to the Rh active center, leading to a rapid decrease in H_2/CO syngas yield even with low sulfur species content, resulting in catalyst poisoning deactivation. The process of metal catalyst poisoning and deactivation involves sulfur compounds adsorbing on the catalyst surface and occupying the active metal sites or forming new non-catalytically active substances, forming stable metal-sulfur bonds, meaning the altered catalyst cannot function properly in DMR reactions [57]. Catalysts cannot be regenerated in case of sulfur poisoning at low temperatures [58]. However, at temperatures above 800°C , the sulfur poisoning of metal catalysts can be reversed to a large extent by removing sulfur-containing compounds [59]. The difficulty of the sulfur poisoning of metal catalysts depends on their physical and chemical properties, such as the properties of active metals, metal-sulfur interactions, and sulfur-support interactions. Gaillard et al. prepared a molybdenum-based catalyst

supported by $\gamma\text{-Al}_2\text{O}_3$ via the constant volume impregnation method and investigated the sulfur resistance of the catalyst supported by Mo and Ni additives. The results show that Ni and Mo catalysts are easy to be deactivated when 50 ppm H_2S is added to the feed gas, and bimetallic Ni-Mo catalysts exhibit better sulfur resistance than single metal catalysts. Ni plays an auxiliary role in Mo-based catalysts, which is related to the preferential adsorption of H_2S on the auxiliary catalysts. The interaction between metal Ni-sulfur was strengthened, thus protecting the Mo active site [60].

4. Study on Restraining of Deactivation of Metal Catalysts in DRM Reaction

The deactivation of metal catalysts in the DRM is the main obstacle hindering their industrial development and application. Catalyst research is the key element in addressing the deactivation issues. To mitigate the deactivation caused by coke deposition, sintering, and sulfur poisoning in the DRM process, some techniques and methods can be employed to effectively alleviate these problems from three aspects: active components, supports, and promoters of the catalyst (as shown in Figure 5). From the aspect of the catalyst metal active component, adjusting the size of the metal active component of the catalyst and thus increasing the reactive sites, and using the synergistic effect of bimetals, can reduce the generation of carbon deposition and accelerate the decarbonization rate of the catalyst. From the aspect of catalyst support, adjusting the acidity and basicity of the catalyst support surface, enhancing the interaction between the support and metal activity, increasing the specific surface area of the support, and changing the shape of the catalyst can restrain the deactivation of the catalyst. In particular, the construction of some specially shaped catalysts can achieve the effect of suppressing catalyst deactivation by using the domain-limiting effect of the support on the metal active component. In terms of catalyst promoters, the addition of a promoter can improve the anti-deactivation ability of catalysts by adjusting the catalyst surface acid-base and metal-support interactions, and the electron density of active metal atoms.

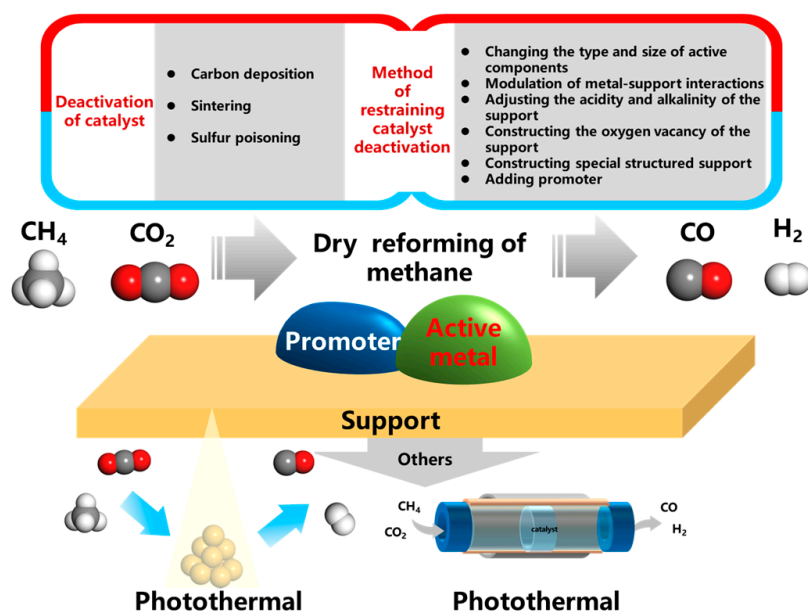


Figure 5. The scheme of the dry reforming of methane.

4.1. Changing the Type and Size of Active Components

The performance of catalysts in the DRM reaction depends on the type of metal active component and particle size used. Compared to transition metal catalysts, precious metal catalysts exhibit higher activity and selectivity, good stability, and better resistance to carbon deposition in the DRM. Nematollahi et al. [61] studied the reaction of the DRM to syngas over $\text{Al}_2\text{O}_3\text{-MgO}$ -supported noble metal catalysts (Rh, Ru, Pt, Pd, and Ir) and all of

the catalysts showed high stability. The BET measurement results indicate that the specific surface area of Ru-, Rh-, and Pd-based catalysts is higher than that of Ir- and Pt-based catalysts. The results showed that the Rh and Ru catalysts had higher activity and the order of activity of the different catalysts was Rh ~ Ru > Ir > Pt > Pd. Caprariis et al. [14] prepared three ternary chalcogenide oxides $\text{BaZr}_{(1-x)}\text{Me}_x\text{O}_3$ via a modified citrate method using noble metals Rh, Ru, and Pt as the active species and investigated their performance in the DRM process. The experimental results showed that the activity of the catalysts increased with the loading of the active species in the order of Rh > Ru > Pt. This is in general agreement with the results of Nematollahi et al. The catalytic activity of Pt was low at temperatures below 923 K. The samples containing Rh and Ru had better catalytic activity, which was related to their high reducing properties. No deactivation of the Rh and Ru catalysts was detected in the test that lasted for a long time, while the activity decreased due to the significant carbon formation rate on the BaZrPtO_3 sample. The chalcogenide LaAlO_3 catalysts were synthesized by Anil et al. via the solution combustion method using Ru, Pt, and Pd as the active species [30]. The catalytic activity of $\text{LaAl}_{0.98}\text{Ru}_{0.02}\text{O}_{3-\delta}$ was higher than that of $\text{LaAl}_{0.98}\text{Pt}_{0.02}\text{O}_{3-\delta}$ and $\text{LaAl}_{0.98}\text{Pd}_{0.02}\text{O}_{3-\delta}$ and showed stable conversion in the stability experiment for 50 h. The catalytic activity of $\text{LaAl}_{0.98}\text{Ru}_{0.02}\text{O}_{3-\delta}$ was higher than that of $\text{LaAl}_{0.98}\text{Pt}_{0.02}\text{O}_{3-\delta}$ and $\text{LaAl}_{0.98}\text{Pd}_{0.02}\text{O}_{3-\delta}$. This is due to the strong interaction between Ru and Al, which leads to the high stability and anti-deactivation performance of this catalyst. Understanding the key active sites in the DRM reaction can help in the study of anti-deactivation. Yentekakis et al. [62] investigated the effect of three oxides with different oxygen storage capacities and stability ($\gamma\text{-Al}_2\text{O}_3$, $\text{Al}_2\text{O}_3\text{-CeO}_2\text{-ZrO}_2$ (ACZ), and $\text{Ce}_2\text{O}_3\text{-CeO}_2$ (CZ)) loaded with noble metal Rh catalysts on DRM reactivity, selectivity, resistance to carbon deposition, and anti-aging. XPS analysis revealed that the main Rh species detected was Rh^0 , and its relative content followed the order of Rh/CZ (100%) > Rh/ACZ (72%) > Rh/ $\gamma\text{-Al}_2\text{O}_3$ (55%), which is consistent with the order of catalytic activity performance. This also indicates that Rh^0 is the key active site, which is beneficial for suppressing the deactivation of the catalyst. In addition, the presence of CZ in the support helps to keep Rh in the metallic state and minimize carbon deposition under the reaction conditions. Jiménez et al. [63] prepared a Pd/CeO₂ (PdAcCeO₂M) catalyst using mechanical force chemistry, which exhibited a unique reaction mechanism and higher DRM reactivity and resistance to carbon deposition compared to Pd/CeO₂ (PdCeO₂IW) catalysts synthesized via conventional impregnation. It was found that the enhanced chemistry of PdAcCeO₂M can be attributed to the presence of carbon-modified Pd⁰ and Ce^{4+/3+} surface arrangements, where the unique Pd-CO intermediate species and strong Pd-CeO₂ interactions are fully activated and sustained under the reaction conditions. This unique arrangement leads to a highly selective and unique surface reaction pathway and a preference for the direct oxidation of CH_x to CO in the reaction. The properties of the catalyst surface were also confirmed via DFT analysis, indicating that the active phase is a partially oxidized Pd^{δ+} modified by the neighboring carbon, forming a unique Pd structure. Compared with PdCeO₂IW under the same reaction conditions, PdAcCeO₂M has a stronger affinity for carbon generation, again indicating that the carbon-modified Pd is a favorable active center for the DRM, reducing the effect of carbon deposition on the catalytic performance.

A large amount of the literature has reported that the development in bimetallic alloy catalysts plays an important role in restraining sintering and carbon deposition in the DRM. Because of the high price of precious metals, their industrial applications are greatly limited. Researchers have introduced small amounts of noble metals into Ni-based catalysts, which not only improve the dispersion of active Ni species and enhance their reactivity but also have strong resistance to carbon deposition. Li et al. [64] prepared Ni/5LSBA-160 and NiPt/5LSBA-160 nanocatalysts for the DRM on a new mesoporous high specific surface area of the LaFeO₃-SBA-15-CTA support. The results showed that the introduction of Pt onto the Ni/5LSBA-160 catalyst enhanced the interaction between Ni and the support, improved the dispersion of the active Ni species, and led to a higher

syngas generation rate. Additionally, the NiPt/5LSBA-160 catalyst exhibited improved resistance to carbon deposition and sintering. The metal Ni can form alloys with other transition metals, effectively changing the surface properties of active metal species, resulting in better catalytic performance and resistance to deactivation, a phenomenon known as the synergistic effect. Zambaldi et al. [65] prepared NiCu bimetallic catalysts for the DRM reaction, which formed NiCu alloys with high activity and lower carbon deposition compared to Ni catalysts. Sokefun et al. [66] prepared Ru-NiMg/Ce_{0.6}Zr_{0.4}O₂ catalysts with different metal loadings using a primary wet process. The reduction capacity and conversion of the catalysts increased with an increase in Ru content. The temperature of X₁₀CH₄ decreased from 807 to 803 °C with the addition of 0.02Ru-NiMg/Ce_{0.6}Zr_{0.4}O₂ and further decreased to 442 °C in 0.32Ru-NiMg/Ce_{0.6}Zr_{0.4}O₂, indicating that the addition of Ru improved the catalytic activity of the catalyst. With an increase in Ru loading, the enhancement of catalyst conversion is attributed to the increased active sites and synergistic effect between Ru and Ni, thereby weakening the interaction between Ni and Mg.

The active metal particle size has a great influence on the performance of the supported catalyst, and both the catalytic efficiency of metal atoms and the anti-deactivation performance increase with decreasing particle size and particle size distribution. Huang et al. [67] successfully synthesized hydrotalcite Ni-Ir/Mg(Al)O catalysts with different Ir/Ni molar fractions using a one-step co-precipitation method. It was found that the addition of Ir facilitated the formation of smaller Ni particles and improved the anti-carbon deposition performance of the catalysts. Liu et al. [68] prepared the Cu-Ni/LSCM catalysts using the impregnation method and showed good catalytic activity and stability in the DRM process. Among the four catalysts with different Ni and Cu atomic mass ratios, the average particle sizes of the active particles of the samples were 46.5, 43.6, 35.7, and 39.9 nm, respectively, as derived from the field emission scanning electron microscopy (FE-SEM) results (e.g., Figure 6). After the activity test, it was found that the smaller the active particle size and the larger the specific surface area, the higher the catalytic activity, leading to higher CH₄ and CO₂ conversions. Chaudhary et al. [69] investigated the catalytic effect of Ni-Al₂O₃ catalysts synthesized under different roasting temperatures for the DRM. It was found that the NiAl-500 catalyst exhibited a higher conversion and yield during DRM and less carbon deposition due to the properties of a smaller particle size and higher Ni⁰ dispersion. In contrast, NiAl-850 had a larger Ni⁰ particle size, lower conversion and yield, and deposited more carbon. A series of Ni/La₂O₃ catalysts were synthesized by Sorcar et al. [70] using nitrogen-rich nickel precursors with different ligand molecular structures. The Ni loading of the catalysts was analyzed using inductively coupled plasma emission spectroscopy (ICP-OES), and the results showed that compared to Ni-BT-C (24.72 wt.%), Ni-DAG-C (23.36 wt.%), and Ni-Gu-C (32.12 wt.%), the catalytic performance of the Ni-AT-C catalyst (18.74 wt.%) was lower. Although Ni-Gu-C had the highest Ni wt.%, the large size and poor dispersion of Ni particles in the resulting catalysts made its performance inferior to that of Ni-BT-C and Ni-DAG-C. Single-atom catalysts (SACs) can minimize the metal particle size and 100% atom utilization, thus improving the reaction performance and anti-deactivation performance. Tang et al. [71] successfully anchored two sets of Ni₁ and Ru₁ monoatomic sites on the surface of CeO₂ nanorods to form a catalyst with Ce_{0.95}Ni_{0.025}Ru_{0.025}O₂ dual monoatomic sites and confirmed the synergistic effect of the Ni₁ and Ru₁ monoatomic sites anchored on the surface of CeO₂, as well as the high activity of CO₂ and CH₄ conversion with the atoms remaining monodispersed and in the cationic state during the catalytic process at 600 °C. Akri et al. [72] synthesized Ni single-atom catalysts dispersed on hydroxyapatite (HAP) via the strong electrostatic adsorption (SEA) method, exhibiting a high reaction rate and good anti-coking performance. Table 2 summarizes the performance of some metal catalysts used for the DRM.

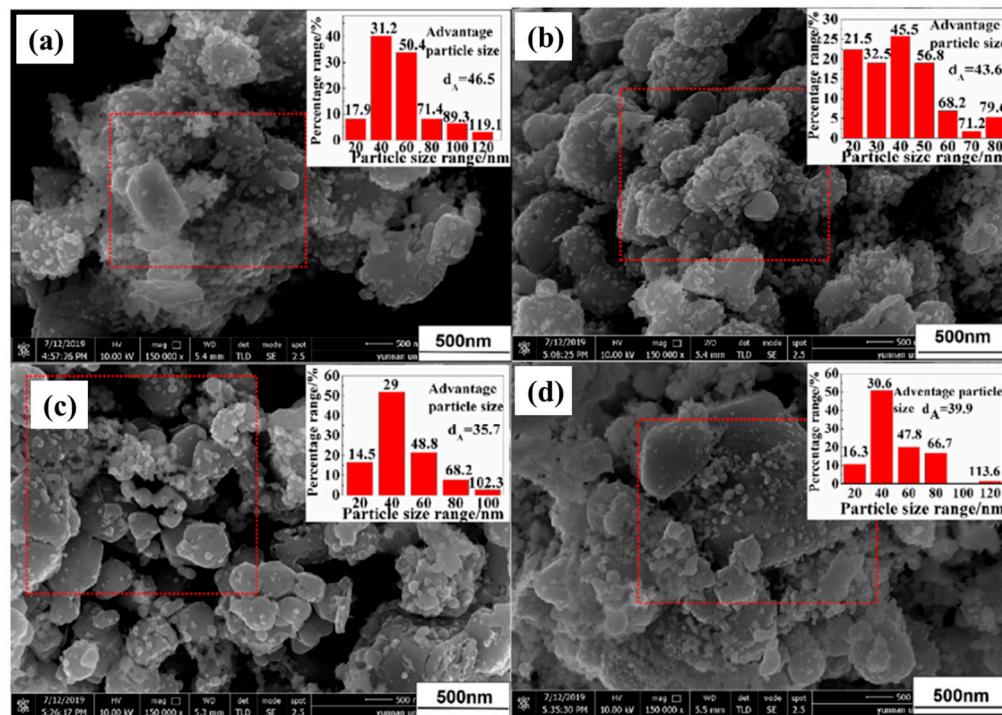


Figure 6. FE-SEM images of fresh Cu-Ni/LSCM with different Ni/Cu mass ratios: (a) 1; (b) 2; (c) 3; (d) 4 [68].

Table 2. Metal catalysts used for the DRM.

| Catalyst | Surface Area (m ² ·g ⁻¹) | GHSV (mL·g ⁻¹ ·h ⁻¹) | Temperature (°C) | Conversion (%) | | Carbon Formation (%) | Reference |
|--|---|---|------------------|-----------------|-----------------|----------------------|-----------|
| | | | | CO ₂ | CH ₄ | | |
| Pt/CeZr/Al ₂ O ₃ | 118 | 6000 | 800 | 68 | 76 | 0.12 | [73] |
| Pt-Ni-CeZrO ₂ | 44 | 5100 | 800 | 54 | 80 | 4.23 | [74] |
| Pt/Mg _{0.85} Ni _{0.15} O | 5.44 | 15,000 | 900 | 76 | 95 | - | [75] |
| 0.2Pd/5Ni-MgO | 181 | 72,000 | 750 | 97 | 96 | 1.5 | [76] |
| 20Mo10Ni/Al ₂ O ₃ | - | 5400 | 800 | 70 | 88 | - | [77] |
| α-MoC _{1-x} | 29.4 | 6000 | 900 | 87 | 94 | - | [78] |
| Rh/SiO ₂ -TiO ₂ | 315 | 6000 | 600 | - | - | - | [79] |
| Rh/Al ₂ O ₃ | 191.8 | 6000 | 700 | 53 | 63 | - | [80] |
| Rh-P/LA | 139 | - | 850 | 90 | - | - | [56] |
| Ru/ZnLaAlO ₄ | 60 | 10,500 | 800 | 89.2 | 90 | - | [81] |
| LaAl _{0.98} Ru _{0.02} O _{3-δ} | 4.0 | 6000 | 800 | 86 | 80 | - | [30] |
| Ir/Ce _{0.9} La _{0.1} O ₂ | 73.9 | 18,000 | 800 | 75 | 85 | 0.23 | [82] |
| Ni-Ir/SiO ₂ | 561.41 | 1200 | 700 | - | 44 | - | [83] |
| Ni/Al ₂ O ₃ | 75 | - | 750 | 81.7 | 95.3 | 0.7 | [84] |
| Ni/CeO ₂ -MgO | 30.6 | 36,000 | 900 | 98.9 | 97.6 | - | [85] |
| Co/SiO ₂ | 194.5 | 20,000 | 850 | 45.02 | 22 | 2.75 | [86] |
| Co/MgO | 51.76 | 24,000 | 750 | 88 | 82 | 0.72 | [87] |

In summary, good stability and anti-deactivation performance can be achieved by changing the active component species and the size of the metal catalysts. Compared to transition metal catalysts, noble metal catalysts exhibit high activity and anti-deactivation performance in methane dry reforming, but are more susceptible to sulfur poisoning. Bimetallic catalysts can effectively change the surface properties of the active metal species, form synergistic effects, and have better anti-deactivation performance. The smaller the particle size of the active component of the metal catalyst, the larger the surface area, the greater the contact area between the reactants and the catalyst, and the faster the reaction

rate, reducing the formation of carbon. Adjusting the particle size has become one of the important means for enhancing the anti-deactivation performance of DRM catalysts.

4.2. Modulation of Support's Physical and Chemical Properties

The support in catalysts has a significant impact on their physicochemical properties. The support affects the catalyst performance by providing attachment sites for the metal active component or interacting with it. In addition, the morphology, pore structure, oxygen vacancies, acidity, and basicity of the support affect its catalytic performance and resistance to deactivation, etc. The DRM reactions generally need to be carried out at higher temperatures, which requires catalyst support with high thermal stability. The reported metal catalyst support is divided into metal oxide support, composite support, and novel support according to the type of support, such as Al_2O_3 , CeO_2 , SiO_2 , TiO_2 , Al_2O_3 - MgO , MgAl_2O_4 , hydrotalcite, chalcocite, and carbon materials.

4.2.1. Modulation of Metal–Support Interactions

During the DRM reaction, two types of interactions occur on the metal catalyst: (i) the interaction between the active metal and the support, or (ii) the effect of the complex interaction between the bimetal and the support. Under certain conditions, by adjusting the interaction between the metal and the support, the particle size and dispersion of the active metal component of the catalyst can be changed, which in turn affects the catalyst's activity and anti-deactivation performance [17]. Strong bonding at the interface between the metal and the support can restrain the sintering of the metal active components and carbon deposition from hydrocarbon reforming, which is known as a strong metal support interaction (SMSI), and can be increased to restrain carbon deposition and metal sintering by increasing SMSI [88]. SMSI also restrains the thermal limitation caused by Hüttig and Tamman temperatures, thus suppressing the sintering of metal active components [89]. SMSI is significantly influenced by heat treatment and reduction conditions during catalyst preparation [90]. SMSI is diminished by a reduction in metal doping sites in the support oxide and usually deactivates the catalyst by encapsulating the active site through these processes. In order to retain SMSI near the active site and increase the catalytic activity of the metal catalyst, the number of surface metal doping sites between the metal and the support must be increased. Jeon et al. [91] proposed a mild reduction process using CH_4/CO_2 gas that restrains the sintering of metal nanoparticles and increases the exposed interface between the metal and the support, Ni and cerium oxide. The results showed that the mild reduction conditions led to the formation of a large amount of the Ni^{3+} phase on the catalyst surface, expanded the interface of SMSI in the catalyst, and significantly restrained the sintering of the catalyst, resulting in a long-term stable operation with high catalytic activity. Kwon et al. [92] prepared Ni/ Al_2O_3 catalysts of different nickel oxide phases, namely NiO and NiAl_2O_4 , by changing the calcination temperature. The results show that the catalytic activity, selectivity, stability, and anti-coking performance of the Ni/ Al_2O_3 catalyst driven by the NiAl_2O_4 phase to the DRM are better than those of the Ni/ Al_2O_3 catalyst driven by the NiO phase. This is because the NiAl_2O_4 precursor is completely reduced at a high temperature ($>950\text{ }^\circ\text{C}$), which strengthens the interaction with alumina, making the Ni particles of the Ni/ Al_2O_3 catalyst more dispersed and smaller in size, thereby improving the catalytic DRM reactivity, which can effectively restrain carbon formation. Duan et al. [93] added Co to Ni/ $\text{Mg}(\text{Al})\text{O}$ via co-precipitation, where the interaction between Ni/Co oxides and MgO slowed down the reduction of Ni and generated small and uniformly dispersed Ni particles. The bimetallic synergistic effect enhanced the complex interaction between the bimetal and the support as well as the dispersion of the metal active component, and provided additional active centers that enhanced CO_2 adsorption at the metal–support interface and promoted the removal of deposited carbon species, thus reducing carbon deposition.

4.2.2. Adjusting the Acidity and Basicity of the Support

The carbon species formed by CH₄ cleavage are formed on the acidic sites of the support. Therefore, regulating the acidity and basicity of the support plays a crucial role in restraining the generation of carbon deposition in the DRM. Alkali and alkaline earth metals are widely used as a support or promoters that reduce the acidity of the support and thus the rate of hydrocarbon cleavage. In addition, increasing the basicity of the catalyst promotes the activation of weakly acidic CO₂, which oxidizes the surface carbon species. The presence of activated CO₂ on the catalyst surface restrains the formation of the carbon species from the CH₄ cracking reaction, thereby increasing the catalyst's resistance to deactivation. Das et al. [94] investigated the correlation between the properties of support acidity and catalyst activity and deactivation by synthesizing Ni-based catalysts using SiO₂ and Al₂O₃ with acidity and basicity as the support. The results showed that too many strongly acidic sites on the support would promote the dehydrogenation of CH₄ cleavage to produce carbon species, leading to the deactivation of the catalyst due to carbon deposition. Although alkaline catalysts can restrain the formation of carbon deposition, too many strong alkaline sites can cause metal oxidation and the Boudouard reaction, which lead to catalyst deactivation. The uniform distribution of moderately acidic and basic centers on the catalyst surface plays a crucial role in the activity, stability, and anti-deactivation ability of the catalyst, which can make the rate of carbon species production from the CH₄ cracking reaction comparable to the rate of carbon species oxidation via surface oxygen, and the smaller Ni particles and SMSI in the catalyst help the catalyst to obtain higher activity, which is conducive to the occurrence of the DRM reaction and restrains catalyst deactivation. Therefore, moderately acidic and basic support can be designed to restrain the deactivation of DRM catalysts as much as possible. Huang et al. [95] prepared Ni-based catalysts via hydrothermal synthesis using S-1 molecular sieves with Lewis acid sites as the support and showed that the balance between the formation and consumption of carbon species in Ni@S-1 with Lewis acid sites (basic sites) is a key step in order to achieve efficient CO₂-CH₄ dry reforming, which is beneficial for restraining the formation of carbon deposition. Jafarbegloo et al. [96] prepared Ni-based catalysts using alkaline oxide MgO as a support via a one-step method and showed that the generation of NiO-MgO solid solution with an alkaline surface was beneficial for restraining the formation of carbon deposition. Because CO₂ is acidic in its essence, the higher the basicity of the support, the more CO₂ is adsorbed, promoting the formation of CO and restraining the formation of carbon deposition. Ghodke et al. [97] synthesized Ti- and Zr-substituted Gd₂B_{2-x}Ni_yO_{7-δ} (B = Ti, Zr) catalysts for the DRM reaction performance research using the citric acid gel method. The research showed that GTNO has strong basicity, which is conducive to CO₂ adsorption and activation, showing higher reactivity and stability. Cao et al. [98] prepared Co/Al₂O₃ and Dy-Co/Al₂O₃ catalysts and performed DRM activity tests at 923~1023 K. The results showed that the Dy-Co/Al₂O₃ catalyst had higher activity, and its superior performance was attributed to the strong adsorption capacity of the basic center of the catalyst for CO₂ and the stronger interaction between Co and Dy. Sengupta et al. [99] used Al₂O₃, CaO-Al₂O₃, MgO-Al₂O₃, etc., as supports to prepare nickel-based catalysts for the study of the DRM reaction performance. The research showed that the Ni and Ni-Co catalysts supported by CaO-Al₂O₃ had additional basic sites. This is beneficial to the chemical adsorption of CO₂ and H₂ and reduces the amount of carbon deposition.

4.2.3. Constructing the Oxygen Vacancy of the Support

Oxygen vacancies are inherent defects formed on the surface of metal oxide catalyst support under high temperatures and low atmospheric pressures [100]. This property of the catalyst support enables it to store O₂ under oxidative conditions and release O₂ under reducing conditions, thereby generating and replenishing O₂ [101]. Supports are usually made of materials with strong oxygen storage capacity (OSC), as they enhance the mobility of O atoms in the lattice and facilitate the generation of oxygen vacancies when interacting with active metals. Oxygen vacancies have the potential to activate and

decompose CO_2 , generating mobile reactive oxygen species on the catalyst surface. The reaction of active oxygen and carbon can generate CO and intermediate carbonate species, which can significantly reduce the formation of carbon deposits [102]. Sophiana et al. [103] used super-OSC CeO_2 and ZrO_2 as supports for Ni-based catalysts, and the results showed that the catalysts had a strong anti-carbon deposition ability. This is due to the fact that the combination of high-OSC CeO_2 and ZrO_2 with Ni increases the mobility of O atoms through the lattice and promotes the formation of oxygen vacancies in the catalyst, and a large number of oxygen vacancies provide sites for CO_2 activation and C-O bond breaking, thus reducing the deactivation of the catalyst due to carbon deposition. Lanre et al. [104] synthesized $\text{CeNi}_{0.9}\text{Zr}_{0.1}\text{O}_3$ catalysts with abundant oxygen vacancies and high activity. It was shown that surface oxygen vacancies are the main cause of methane activation. Ce has sufficiently high oxygen storage capacity and high lattice oxygen mobility, helping it to improve catalytic performance. The addition of an appropriate amount of Ce can increase oxygen vacancies, which can activate oxygen-containing compounds to react with carbon species and eliminate carbon deposition. In addition, the redox cycle between Ce^{3+} and Ce^{4+} contributes to the leaching of carbon deposited on the catalyst through oxygen vacancies. Owgi et al. [105] similarly synthesized Ni/FSA catalysts with abundant oxygen vacancies and a high specific area. The high specific surface area provides the catalysts with higher OSC and more oxygen vacancies, which can oxidize carbon species to CO and form intermediate carbonate substances on reducible alkaline support, thus avoiding the formation of carbon deposition. Oxygen vacancies play a crucial role in improving the physicochemical properties of metal oxide catalysts by tightly binding CO_2 and promoting CO_2 adsorption, activation, and dissociation in the DRM. Zhu et al. [106] synthesized the Ni/ Al_2O_3 - Y_2O_3 -3% Nd_2O_3 catalyst via the sol-gel method, and the experimental results showed that Ni/ Al_2O_3 - Y_2O_3 -3% Nd_2O_3 exhibited excellent activity and stability at 800 °C which was attributed to the catalyst having sufficient oxygen vacancies to restrain the formation of Ni sintering and carbon deposition. The addition of Nd_2O_3 promoted the formation of oxygen vacancies in the catalyst, facilitating the decomposition of CO_2 into CO and O^* species, and the resulting O^* would react with the deposited carbon in time, avoiding the formation of low-activity graphitic carbon and restraining carbon deposition. Wang et al. [107] prepared Ni-In/ γ - Al_2O_3 catalysts using a “two-solvent” method, and the addition of In increased the number of adsorbed oxygen species and oxygen vacancies on the Ni/ Al_2O_3 catalyst surface, which act as active sites for CO_2 chemisorption to generate reactive CO_2 , making it easier for reactive CO_2 to form a carbonate. It also reacts with the deposited carbon to generate CO, eliminating carbon deposition on the catalyst and restraining catalyst deactivation.

4.2.4. Constructing Special Structured Support

Mesoporous materials are porous materials with pore sizes in the range of 2–50 nm. They are used in a variety of catalytic reactions because of their consistent and cohesive porous structure and high specific surface area, which are conducive to the uniform dispersion of active components and the adsorption of reactants when used as a support, and can be selected according to the appropriate pore size for different reactions to reduce the diffusion resistance of reactants and products, which is conducive to the formation of strong metal-support interactions and prevents the sintering and carbon deposition of catalysts. MCM-41, first synthesized by researchers at Mobil Oil, is a two-dimensional hexagonal material with uniform hexagonal pore channels and a pore size generally in the range of 2–10 nm. MCM-48 has a uniform pore size of about 2.6 nm and two sets of mutually independent three-dimensional helical surface pore channels, while MCM-50 is a mesoporous material with a laminar structure. They all have a large specific surface area, ordered pore structure, controllable and adjustable pore size, and good thermal stability. SBA-15 also has a two-dimensional hexagonal structure, and its pores are generally 5–10 nm. Compared with MCM-41, SBA-15 has a thicker pore structure and higher hydrothermal stability, and a rougher surface is conducive to the dispersion of metal active components [108,109].

Ordered mesoporous materials such as MCM-41 and SBA-15 are often used as a support for the DRM reaction catalysts. Zhang et al. [110] prepared Ni-SBA-15 and Ni-MCM-41 catalysts using a solid-state grinding method and found that Ni-SBA-15 exhibited higher catalytic activity and thermal stability in the DRM reaction. This is due to the larger pore size of the Ni-SBA-15 catalyst compared to the Ni-MCM-41 catalyst, which makes it easier for the Ni particles to disperse inside the SBA-15 support, thus increasing the Ni dispersion sites. Similar conclusions were also drawn by Liu et al. [108]. Due to the uniform and ordered mesopore distribution and unique pore structure of SBA-15, the catalytic performance of Ni-SBA-15 is better than that of Ni-MCM-41. Additionally, the nanometer-scale linear hexagonal pores of SBA-15 can effectively limit the growth of metal particles, thereby contributing to the dispersion of active metal components, restraining the sintering of active metal components, and preventing catalyst deactivation [111]. Zhu et al. [112] investigated the effects of $\text{La}_{0.7}\text{Sr}_{0.3}\text{AlO}_3$ and SBA-15 support on the activity and durability of Ni-based catalysts in the DRM. The results showed that SBA-15 has better resistance to carbon deposition than $\text{La}_{0.7}\text{Sr}_{0.3}\text{AlO}_3$, which is due to the regular ordered pore structure of SBA-15 which can make the Ni particles well dispersed and restrain the agglomeration of Ni particles, thus making it have better catalytic performance in the DRM. The zeolite molecular sieve is also a mesoporous material with a unique regular crystal structure and a large specific surface area. Most zeolites have certain acidic centers and a good affinity for CO_2 gas, and they can promote the dispersion of metal particles to some extent. Because of these properties, zeolite molecular sieves have been widely used in catalytic DRM reactions in recent years. Moradi et al. [113] compared the activity of some Ni/ZSM-5 catalysts with different silica/alumina ratios for the DRM reaction. They found that Ni/ZSM-5 catalysts possessed the highest catalytic activity and thermal stability when the silica/alumina ratio reached 30. In addition to the structural advantages of the mesoporous material, the special chemical structure of its surface can also enhance the interaction between its active metal components and the support. Zhang et al. [110] preserved the silica hydroxyl species in the pore channel of SBA-15 by adjusting the calcination sequence. The silica hydroxyl species had a strong anchoring effect on the Ni particles, which strengthened the interaction between Ni and SBA-15 support and resisted the sintering of Ni metal particles, thus restraining the deactivation of the catalyst.

Nanofibers, nanorods, and nanoparticle-shaped catalysts can reduce the size of metal particles and improve their dispersion, thus providing more active sites to speed up the reaction rate and achieve a reduction in carbon deposition. Many researchers have found that the physicochemical properties of nanorods depend on their size, and the developed catalysts exhibit significant catalytic activity and thermal stability [114]. The results show that the nanorod-like structure formed by cerium dioxide can provide good support for the DRM due to the ability of the nanorod-structured catalyst to accelerate carbon precursor vaporization and reduce sintering by enhancing the interaction between the loaded metals. Wang et al. [82] compared the effect of Ir catalysts loaded on $\text{Ce}_{0.9}\text{La}_{0.1}\text{O}_2$ nanorods (as shown in Figure 7) and nanoparticles in the DRM reaction to syngas. It was found that due to the exposure of active {110} and {100} crystalline surfaces in the $\text{Ir}/\text{Ce}_{0.9}\text{La}_{0.1}\text{O}_2$ nanorod catalysts, the exposure of these crystalline surfaces facilitated an increase in the surface area of the catalyst, an increase in the number of pore channels, and enhanced metal-support interactions, and had stronger redox properties and more oxygen vacancies than the $\text{Ir}/\text{Ce}_{0.9}\text{La}_{0.1}\text{O}_2$ nanoparticle catalysts that promoted the activation and conversion of CH_4 and CO_2 . These reasons contribute to the Ir metal particle size maintenance, reducing the amount of carbon deposition and restraining the deactivation of the catalyst. This work demonstrates that the support morphology has a significant effect on the catalyst activity in the DRM reaction. González et al. [115] prepared DRM catalysts with high catalytic activity and stability using nanoparticulate, nanofibrous alumina as a support loaded with Ni, the active component of Ni-Ce. The support morphology and Ni-Ce bimetallic effect in Ni-based alumina catalysts were investigated in the DRM. It was shown that the morphology of alumina has an important effect on the preparation of alumina-based

catalysts with high catalytic activity. The morphology effect is related to the mesoporosity, and higher pore size presented by nanofibrous alumina, which improves the diffusion of Ni-Ce precursors in the impregnation step and facilitates the formation of smaller-sized metal particles as well as the dispersion of metal particles. On the other hand, Ni-Ce incorporation has a similar effect on the fiber morphology, which reduces the Ni particles' size and improves their dispersion. Nanofiber morphology catalysts can use the size and number of pore channels to limit the size of metal particles and prevent the sintering of the catalyst under high temperatures. Wang et al. [83] introduced NiO nanoparticles onto the SiO₂ surface before adding Ir sources to the bimetallic Ir-Ni/SiO₂ catalyst, and the uniform NiO nanoparticles provided limited loading vacancies to prevent the agglomeration of Ir nanoparticles under hydrogen reduction. The Ir-Ni/SiO₂ catalyst consists of ultrasmall bimetallic nanoparticles (1.4 nm) uniformly distributed on the SiO₂ surface, composed of the bimetallic nanoparticles. Due to the synergistic effect within the bimetals, the prepared bimetallic catalysts showed significantly improved catalytic performance for the DRM reaction, which was 1.2 times higher than the sum of Ir and Ni monometallic catalysts. In addition, the side reactions of the inverse water gas conversion reaction were effectively suppressed and the catalyst stability was improved. The nanoparticle-shaped catalysts, on the other hand, reduce the agglomeration of metal particles by restricting the loading vacancies of the catalysts and improving the catalytic activity for the DRM.

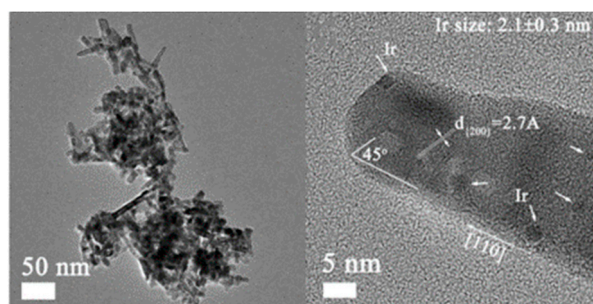


Figure 7. Ir/Ce_{0.9}La_{0.1}O₂ nanorods [82].

The core-shell framework catalyst is a kind of catalyst with a special structure. Different from the loading forms of the active component and the support in common catalysts, the core-shell catalyst is wrapped onto a metal active component via a special preparation method which uses the strong interaction between the support and the active component, as well as the restricted domain effect of the support on the active component, to restrain the sintering of the catalyst under a high temperature, and also blocks the growth space of filamentous carbon C_β, restrains the formation of carbon deposition, improves the catalytic activity and thermal stability of the catalyst, and prevents the deactivation of the catalyst. Peng et al. [116] prepared a multi-core Ni@SiO₂ catalyst with a Ni particle size of 4.3 nm using a one-pot reverse microemulsion method. Due to the small size of the Ni particles and the confinement effect of the shell, the catalyst exhibited excellent activity and resistance to carbon deposition during the reaction. After a reaction evaluation at 800 °C for 100 h, the conversion rates of CH₄ and CO₂ remained above 90%. Li et al. [117] synthesized a series of Ni@SiO₂ and Ni-yolk@Ni@SiO₂ catalysts with different shell thicknesses. By comparing their catalytic performance in the DRM reaction, it was found that the Ni-yolk@Ni@SiO₂ catalyst with a shell thickness of 11.2 nm exhibited high activity and thermal stability, with a CH₄ conversion rate of 90% and a CO₂ conversion rate of 95% at 800 °C. When the shell layer thickness of Ni-yolk@Ni@SiO₂ reaches 11.2 nm, the cavity structure that appears inside the catalyst and the pore channels that appear in the central part are favorable for the diffusion of reactants and products. Due to the strong interaction between the active center Ni and the support SiO₂, a certain amount of layered silicate Ni material is formed, and its reduction leads to the formation of “small satellite” Ni particles that can improve the catalyst activity; due to the confinement effect, the core-shell structure

evolves to the “yolk-shell” structure after calcination, which further improves the catalyst activity. Li et al. [118] synthesized $\text{CeO}_2 @\text{Ni-Ps}$ YS catalysts with a yolk-shell structure. SMSI between Ni and Ni-Ps prevented Ni agglomeration under high temperatures, and CeO_2 remained in cubic form due to the protection of the Ni-Ps yolk-shell structure, which restrained the sintering of the CeO_2 nuclei and made it highly resistant to a loss of activity under a high temperature. Similarly, Kim et al. [119] developed a nanotubular eggshell Pt-NiCe@ SiO_2 SAA catalyst with high anti-carbon deposition performance due to its Pt-Ni SAA interaction and yolk-shell morphology. The closed morphology of the yolk-shell structure allows for easier desorption of CO from the surface, thus hindering carbon deposition. The Pt-Ni SAA interaction enhances the reduction of Ni, which further restrains the carbon deposition in the DRM process. Wang et al. [120] then simulated the kinetic parameters of the DRM substrate reaction over the Pt-NiCe@ SiO_2 SAA catalysts and elucidated the effects of eggshell morphology and Pt-Ni SAA on the reaction kinetics. The results show that high O^* and low H^* coverage are observed on Pt-NiCe@ SiO_2 SAA catalysts due to the Pt-Ni SAA interaction and eggshell morphology, both of which can lead to its C^* easy removal and thus stable DRM activity. Additionally, it was found to be more inclined to C^* elimination and rapid CO^* desorption, which also suggests that the reverse Boudouard reaction can prevent catalyst deactivation due to carbon deposition.

Regulating the physicochemical properties of metal catalyst supports is a promising strategy for preventing deactivation in the DRM. By adjusting the strong metal-support interactions, the surface properties of active components, including crystal size, dispersion, and reducibility, can be altered, thereby affecting the catalytic activity and carbon resistance. Tuning the acidity and basicity of the catalyst can mitigate carbon deposition by promoting the activation of weakly acidic CO_2 , which in turn oxidizes surface carbon species and suppresses carbon formation via methane cracking. Oxygen vacancies can activate and decompose CO_2 , generating mobile active oxygen species on the catalyst surface, which can significantly reduce carbon deposition by reacting with carbon to form CO and intermediate carbonate species. Compared to conventional supported catalysts, special morphologies such as mesoporous, nanorod, nanoparticle, and core-shell structures can enhance the metal-support interaction, confine metal particles within a limited domain, increase the number of active sites, and improve the catalyst's resistance to sintering and carbon deposition, thus mitigating catalyst deactivation during the reaction.

4.3. Adding Promoter

Alkali metals, alkaline earth metals, and rare earth metal oxides are commonly used as promoters in the DRM reaction catalysts. The role of La in hydrotalcite-like Ni-based catalysts was investigated by Kalai et al. [121]. The results showed that the addition of La enhanced the interaction between Ni and the support, increased the effective active center, and restrained the inverse water-gas reaction during the reaction. Wang et al. [122] added an appropriate amount of auxiliary La to tungsten carbide-activated carbon (WC-AC)-loaded Co catalysts for the DRM reaction and found that the addition of La auxiliary helped the catalyst to convert Co^{3+} species into active Co^{2+} species, increased the ratio of O_a and O_b in the active component and oxygen species, and restrained the formation of unfavorable CoWO_4 species, thus improving the catalyst activity and resistance to carbon deposition. Seo et al. [123] investigated the auxiliary effects of Mg, Ca, Sr, Ba, and La on Ni catalysts loaded on alumina and found that all of these alkali metals were loaded on the support in the form of small particles and increased the basicity of the support. It was found that the anti-carbon deposition performance of the catalyst could be significantly enhanced by adding a certain amount of Sr, which was attributed to the fact that the addition of Sr could form a strong interaction with Ni, reducing the particle size of Ni particles and hindering the formation of filamentous carbon C_β , resulting in more easily eliminated amorphous carbon C_α . Nisa et al. [124] prepared Ni/MCM-41 catalysts doped with Mg, Ca, Na, and K via the primary wet impregnation method and found that the addition of both Ca and Mg helped to restrain the sintering of the active component Ni

under high temperatures, and Ca and Mg also increased the basicity of the catalyst, which promoted the adsorption of CO₂ and thus reduced the formation of carbon deposition. Zeng et al. [125] used a hydrothermal synthesis method to dope the alkaline additive MgO onto the SiO₂ support and found that the addition of MgO enhanced the basicity of the catalyst surface, resulting in the enhanced ability of CO₂ adsorption on the catalyst surface, which in turn improved the reactivity. On the other hand, the Ni-MgO interface not only improves the distribution of Ni but also promotes the cracking of CH₄ and the activation of CO₂, thus accelerating the elimination of carbon deposition and improving the anti-carbon capacity of the catalyst. The addition of alkali and alkaline earth metals and their oxides can increase the catalyst surface basicity and metal-support interaction, thus improving the adsorption capacity of CO₂ and the anti-sintering and anti-carbon deposition performance of the catalyst.

The addition of a promoter to catalysts not only improves the catalyst acidity and metal-support interaction but also regulates the electron density of the metal atoms of the active component and improves the mobility of the lattice oxygen in the catalyst, thus increasing the dispersion of the active metal component and enhancing the adsorption, dissociation, and activation of CH₄ and CO₂ to improve the reaction efficiency as well as the anti-sintering and anti-carbon deposition of the catalyst.

5. Other Methods to Prevent Deactivation of Metal Catalysts in DRM Reaction

In addition to the solutions of changing the active component size and type, tuning the physicochemical properties of the support, and adding promoters, different reaction-driving methods such as photothermal synergistic catalysis and plasma catalysis are also promising strategies to address the deactivation of metal catalysts in the DRM reaction.

5.1. Photothermal Catalysis

In recent years, carbon-free solar energy, especially concentrated solar energy, has been used for the DRM, and solar-driven photothermal chemical DRM (PTC-DRM), which integrates photochemical and thermochemical processes in a single reaction system, has been developed for the better utilization of solar energy [126]. Unlike thermochemical DRM driven by heat and photochemical DRM driven by light, photothermal catalysis can utilize the energy of lower wavelengths of light in the solar spectrum, combining the advantages of thermochemistry and photochemistry to synergistically drive catalytic DRM reactions, and photothermal oxidation and the reduction of CH₄ and CO₂ are efficient and green catalytic pathways [127]. Du et al. [128] prepared Ni-CeO₂/ZrO₂ photothermal catalysts using ZrO₂ as the support and loaded them with the active component Ni and the additive CeO₂. The results showed that Ni-CeO₂/ZrO₂ exhibited high and stable PTC-DRM activity with an average hydrogen production rate of 713 mmol·g⁻¹h⁻¹ and a CO production rate of 693 mmol·g⁻¹h⁻¹ under 700 °C illuminations. The light effect of CeO₂ is effectively combined with the plasma effect of Ni, which contributes to the elimination of carbon deposition and activity enhancement, and CeO₂ enhances the strong Ni metal-support interaction, enabling the continuous generation of oxygen vacancies under illumination, thus contributing to the slowing of the carbon deposition and facilitating the dissociation of adsorbed intermediates. These findings facilitate the design of efficient catalytic systems that can efficiently convert greenhouse gases into valuable chemicals through solar photothermal chemical catalysis processes. Yang et al. [129] designed a DRM photocatalyst Rh/CeXWO₃ with both photothermal and photoelectric processes, thus overcoming the thermodynamic limitations of the DRM under conventional conditions. The results show that photo-induced metal-to-metal charge transfer plays a key role in the DRM reaction, which leads to redox cycling between the Ce and W species, thus reducing the activation energy. Quantum mechanical studies show that the high oxygen mobility of CeXWO₃ is accompanied by the formation of oxygen-bridged species, leading to a significant elimination of the deposited C species during the reaction. Zhang et al. [130] prepared Pt/mesoporous TiO₂ photothermal catalysts for the DRM reaction. The Pt active components were uni-

formly dispersed on mesoporous TiO_2 with a small size. Quantum-scale Pt nanoparticles and metal–semiconductor structures induced plasmon resonance and SMSI effects, which could broaden the photoresponse range and enhance the absorption of the incident light, which was beneficial for improving the photothermal catalytic performance of the catalyst. Illumination can cause surface plasmon resonance, resulting in high local temperature and a large number of high-energy electrons, enhancing the adsorption and dissociation of CH_4 on the Pt surface. The increase in CO_2 conversion and CO generation after the light introduction is attributed to the photoelectric effect of the semiconductor TiO_2 , where the generated e^- and h^+ are involved in the activation of CO_2 . O^* and h^+ will combine with CH_x^* to produce intermediate products, such as $-\text{HCOO}$, $-\text{OH}$, and CH_x , which are further converted to H_2 and CO. Thus, the thermocatalytically active center of Pt and the photocatalytically active center of TiO_2 together enhance the DRM process. Gao et al. [131] utilized photocatalytic/photothermal catalytic coupling for light-driven and efficient DRM reactions and designed a Pt/ La_2O_3 catalyst capable of absorbing full-wavelength sunlight. Under light irradiation, the local surface plasmon resonance on Pt/ La_2O_3 excites more hot electrons and oxygen vacancies and triggers an increase in the surface temperature of the catalyst, promoting the dissociative conversion of CH_4 to CH_x and H^+ , which are further converted to C^* and H_2 . The light-excited hot electrons also promote the spontaneous desorption of H_2 , restraining the RWGS reaction and further improving the activity and selectivity of the catalyst. CO_2 decomposes to form CO, O^* , or formate intermediates. In addition, CO_2 can react with La_2O_3 to form $\text{La}_2\text{O}_2\text{CO}_3$. O^* and $\text{La}_2\text{O}_2\text{CO}_3$ promote the oxidation of C^* to CO and reduce the generation of carbon deposition. The synergistic effect of the photothermal reaction and photoactivation is the key to the photothermal catalytic DRM process.

5.2. Plasma Catalysis

Plasma technology offers a gas conversion method for the DRM that is easier to operate and has milder reaction conditions than traditional thermocatalytic DRM [132]. Plasma is the fourth state of matter and is a neutral ionized gas with energetic substances such as electrons, photons, ions, atoms, radicals, and excited molecules, which induce DRM reactions by participating in excitation, ionization, and dissociation processes [133]. Energetic species are further divided into light and heavy particles, which have great potential to drive DRM reactions to produce syngas and chemicals. Based on the relative energy levels of electrons and the average gas/electron temperature, plasma technologies can be further divided into two main categories: high-temperature or thermal plasma reforming, and non-thermal plasma (NTP) reforming. NTP is considered to be very promising in the DRM due to its low temperature (150–450 °C) and atmospheric pressure operation, where dielectric blocking discharges (DBD) are non-thermal-plasma-catalyzed and the most widely used [134]. A lot of research has been conducted by domestic and foreign scholars on the combination of non-thermal plasma and multiphase catalysis. The combination of plasma with metal catalysts can improve the conversion of CH_4 and CO_2 , improve the selectivity of products, and improve the stability, anti-sintering, and anti-carbon deposition properties of catalysts. Wang et al. [135] investigated the synergistic effect of the Ni/ $\gamma\text{-Al}_2\text{O}_3$ catalyst and non-thermal plasma on DRM in a DBD reactor. Under plasma conditions, the conversion rates of CH_4 and CO_2 were 11% and 21%, respectively. Under the synergistic effect of the plasma and catalyst with the same experimental conditions, the conversion rates of CH_4 and CO_2 increased by 33% and 22.5%, respectively. The increase in conversion rate is due to the existence of the plasma–catalyst interface, which provides multiple reaction pathways in surface chemistry. Khoja et al. [136] studied the DRM reaction with the addition of the Ni/ $\gamma\text{-Al}_2\text{O}_3\text{-MgO}$ catalyst in a DBD plasma reactor. They found that the energy efficiency of plasma and Ni/ $\gamma\text{-Al}_2\text{O}_3\text{-MgO}$ -catalyzed DRM was higher than that of the pure-plasma-catalyzed DRM reaction, which indicated a synergistic effect between the Ni/ $\gamma\text{-Al}_2\text{O}_3\text{-MgO}$ catalyst and plasma. On this basis, Khoja et al. [137] also synthesized Ni/ $\text{La}_2\text{O}_3\text{-MgAl}_2\text{O}_4$ catalysts and performed DBD plasma DRM tests, and applied regression models to derive

the process parameters that have the greatest influence on the catalytic performance in the order of input power, total feed flow rate, catalyst dosage, and feed ratio. The stronger plasma catalytic performance under optimal conditions was attributed to the properties of Ni/La₂O₃-MgAl₂O₄ with high Ni dispersion, oxidation capacity, and basicity. The high conversion and anti-coking properties are attributed to the high surface area of the catalyst, the properties of the support, and the good dispersion of the active metal. Integrating the catalyst into the discharge zone of DBD plasma can have additional effects on the system efficiency. The plasma-catalyst interface increases the lifetime and collision possibility of active species and enhances surface modification and electric fields. These factors contribute to improving gas treatment in DBD plasma-assisted DRM. DBD plasma has great potential in the DRM to couple with catalysis and electrolysis, and further studies on this technology may eventually lead to commercial applications.

6. Real Applications

Currently, methane dry reforming technology has limited practical applications. In 2017, the Chinese Academy of Sciences successfully developed a “methane-carbon dioxide self-heating reforming synthesis gas production unit” with completely independent intellectual property rights, and achieved the stable operation of the world’s first demonstration unit at the ten-thousand-ton level using Ni-Ca-ZrO₂ catalysts. The team led by Changchun Yu at the China University of Petroleum (Beijing) verified the reliability of the dry reforming catalyst and process technology via a 1000 h methane dry reforming industrial sideline technology verification test, and achieved high dry reforming conversion technology indicators: CH₄ conversion rate above 95%, CO₂ conversion rate above 92%, and product dry gas containing CO ~49%, H₂ ~46%, CH₄ ~1.5%, and CO₂ ~2.5%. Catalyst sintering and coking, leading to deactivation, are currently important factors hindering practical application development. The main research direction is to prevent the active component from sintering under a high temperature and to prevent the reaction from generating coke.

7. Summary

The DRM reaction using CH₄ and CO₂ can enhance the utilization of CH₄ and CO₂ resources, and the syngas produced by the reaction is easier to further react. This makes it a green and environmentally friendly technology for generating syngas of great significance in the fields of chemical industry, energy, and environmental protection, as well as mitigating global climate change and reducing carbon emissions. The DRM reaction has become a research hotspot, but catalyst deactivation is a core problem that needs urgent solutions. The authors reviewed the thermodynamics and reaction mechanism of the DRM reaction, the main causes of the deactivation of metal catalysts in the DRM reaction, the factors affecting the anti-deactivation performance of catalysts, including active components, support, and additives, and the application of metal catalysts in photothermal and plasma-catalyzed DRM to review the progress of catalyst-restraining deactivation research into the DRM reaction in recent years. This provides a reference for the design and development in high-activity and high-anti-deactivation-performance catalysts. All in all, the main conclusions of this paper are summarized as follows:

1. According to the thermodynamic research into the DRM reaction, a high temperature and low pressure are beneficial for the reaction. The basic reaction mechanism of the DRM is generally divided into three steps: CH₄ dissociation, CO₂ dissociation, and intermediate product oxidation. The adsorption and cracking of CH₄ are the rate control steps of the DRM reaction. CO₂ activation plays a key role in restraining carbon deposition. The DRM reactions still have problems of catalyst deactivation due to high-temperature susceptibility to sintering, carbon deposition, and poisoning, which is an important factor currently restraining their development. How to prevent the sintering of metal active components under high temperatures and prevent carbon deposition during the reaction process are the main directions and technical difficulties for future research.

2. Adjusting the size of the metal active component of the catalyst to increase the reactive sites and using the synergistic effect of bimetals can reduce the carbon deposition and accelerate the carbon removal rate of the catalyst. Adjusting the acidity and basicity of the catalyst support surface, enhancing the interaction between the support and the metal activity, increasing the specific surface area of the support, and changing the morphology of the catalyst can restrain the deactivation of the catalyst. In particular, constructing some special morphology of catalysts can enhance the interaction force between the active component and the support, and the domain-limiting effect can limit the migration and dispersion of the active component to prevent metal sintering. It can also reduce the size of metal particles to provide more active sites for the catalyst and reduce the formation of carbon in the reaction. The synergistic effect of the two mechanisms can achieve the purpose of restraining catalyst deactivation, which is the future development direction of developing highly stable catalysts. The addition of additives can improve the catalyst's resistance to deactivation by modulating the catalyst surface acidity and basicity, the metal–support interaction, and the electron density of the active metal atoms.
3. The photothermal catalytic DRM reaction couples to the advantages of thermal catalysis and photocatalysis, which can reduce the reaction temperature in the DRM process and prevent catalyst deactivation under a high temperature. A development in new high-efficiency photothermal catalyst materials is expected to make the DRM process greener and more environmentally friendly. The combination of plasma and metal catalysts improves CH₄ and CO₂ conversion, product selectivity, catalyst stability, sintering resistance, and carbon deposition resistance properties. The plasma–catalyst interface increases the lifetime and collision potential of the active species and enhances surface modification and electric fields. These factors contribute to improved gas handling in DBD plasma DRM.
4. Despite significant success in adjusting the interactions between catalyst components to enhance catalyst performance, there has always been a trade-off between activity and stability. Therefore, in designing stable and efficient DRM catalysts in the future, the synergistic correlations among various parameters must be considered. The successful development in metal catalysts with good activity and long-term stability is the key to industrializing and commercializing synthesis gas production using DRM technology. More advanced characterization methods should be used to study the reaction mechanisms, coking mechanisms, sintering mechanisms, and sulfur poisoning mechanisms of metal catalysts, so as to deeply understand the catalytic reactions and anti-deactivation mechanisms of metal catalysts. In terms of reaction kinetics and mechanisms, the DFT modeling of catalysts should be prioritized to save time and resources in understanding these interactions and their corresponding effects on catalyst performance. High-performance dry reforming metal catalysts should be designed and developed in a theoretical and practical manner. Attempts can be made to provide more active sites for metal catalysts through the combination of bimetallic or multi-metallic synergistic effects with other strategies, such as strong metal–support interactions, confinement effects, surface acid–base properties, oxygen vacancies, etc., to inhibit metal sintering and coking and to improve the catalytic activity and anti-deactivation performance of the catalyst. In addition, various synthetic methods can be explored in combination with different reaction conditions, and advanced synthesis methods such as organic-assisted impregnation, plasma methods, and atomic layer deposition will play an increasingly important role in the preparation of metal catalysts. Different reaction driving methods during the reaction process will be the future direction of catalytic reactions, such as photothermal synergistic catalysis, and the impact of plasma on the structure and reaction process mechanisms of catalysts will become a future research direction.

Author Contributions: Conceptualization, B.Y. and T.Z.; investigation, B.Y. and T.Z.; writing—original draft preparation, B.Y.; writing—review and editing, T.Z., B.Y., Y.H., X.Z., M.W. and C.L. All authors have read and agreed to the published version of the manuscript.

Funding: This work was supported by the National Natural Science Foundation of China (grant no. 52270114), and was funded by the Open Foundation of Shaanxi Key Laboratory of Lacustrine Shale Gas Accumulation and Exploitation (under planning) (no. YJSYZX23SKF0020) and the Fundamental Research Funds for the Central Universities (2022YJSHH12).

Institutional Review Board Statement: Not applicable.

Informed Consent Statement: Not applicable.

Data Availability Statement: Not applicable.

Conflicts of Interest: The authors declare no conflict of interest.

References

1. Abdullah, B.; Abd, G.N.A.; Vo, D.N. Recent advances in dry reforming of methane over Ni-based catalysts. *J. Clean. Prod.* **2017**, *162*, 170–185. [[CrossRef](#)]
2. Nisbet, E.G.; Manning, M.R.; Dlugokencky, E.J.; Fisher, R.E.; Lowry, D.; Michel, S.E.; Myhre, C.L.; Platt, S.M.; Allen, G.; Bousquet, P.; et al. Very Strong Atmospheric Methane Growth in the 4 Years 2014–2017: Implications for the Paris Agreement. *Glob. Biogeochem. Cycles* **2019**, *33*, 318–342. [[CrossRef](#)]
3. Ghaemi, Z.; Smith, A.D. A review on the quantification of life cycle greenhouse gas emissions at urban scale. *J. Clean. Prod.* **2020**, *252*, 119634. [[CrossRef](#)]
4. Pimm, A.J.; Palczewski, J.; Barbour, E.R.; Cockerill, T.T. Using electricity storage to reduce greenhouse gas emissions. *Appl. Energy* **2021**, *282*, 116199. [[CrossRef](#)]
5. Khan, M.N.; Chiesa, P.; Cloete, S.; Amini, S. Integration of chemical looping combustion for cost-effective CO₂ capture from state-of-the-art natural gas combined cycles. *Energy Convers. Manag.* **2020**, *7*, 100044. [[CrossRef](#)]
6. Akri, M.; Chafik, T.; Granger, P.; Ayrault, P.; Batiot-Dupeyrat, C. Novel nickel promoted illite clay based catalyst for autothermal dry reforming of methane. *Fuel* **2016**, *178*, 139–147. [[CrossRef](#)]
7. Németh, M.; Sáfrán, G.; Horváth, A.; Somodi, F. Hindered methane decomposition on a coke-resistant Ni-In/SiO₂ dry reforming catalyst. *Catal. Commun.* **2019**, *118*, 56–59. [[CrossRef](#)]
8. Kaddeche, D.; Djaidja, A.; Barama, A. Partial oxidation of methane on co-precipitated Ni-Mg/Al catalysts modified with copper or iron. *Int. J. Hydrogen Energy* **2017**, *42*, 15002–15009. [[CrossRef](#)]
9. Yentekakis, I.V.; Dong, F. Grand challenges for catalytic remediation in environmental and energy applications toward a cleaner and sustainable future. *Front. Environ. Chem.* **2020**, *1*, 5. [[CrossRef](#)]
10. Yentekakis, I.V.; Goula, G. Biogas management: Advanced utilization for production of renewable energy and added-value chemicals. *Chem. Front. Environ. Sci.* **2017**, *5*, 7. [[CrossRef](#)]
11. Jiang, C.; Loisel, E.; Cullen, D.A.; Dorman, J.A.; Dooley, K.M. On the enhanced sulfur and coking tolerance of Ni-Co-rare earth oxide catalysts for the dry reforming of methane. *J. Catal.* **2021**, *393*, 215–229. [[CrossRef](#)]
12. Gao, N.; Cheng, M.; Quan, C.; Zheng, Y. Syngas production via combined dry and steam reforming of methane over Ni-Ce/ZSM-5 catalyst. *Fuel* **2020**, *273*, 117702. [[CrossRef](#)]
13. Jang, W.; Shim, J.; Kim, H.; Yoo, S.; Roh, H. A review on dry reforming of methane in aspect of catalytic properties. *Catal. Today* **2019**, *324*, 15–26. [[CrossRef](#)]
14. Scarsella, M.; Caprariis, B.D.; Filippis, P.; Palma, V. Rh, Ru and Pt ternary perovskites type oxides BaZr_(1-x)Me_xO₃ for methane dry reforming. *Appl. Catal. A* **2016**, *517*, 47–55.
15. Ma, Y.; Su, P.; Ge, Y.; Wang, F.; Xue, R.; Wang, Z.; Li, Y. A novel LaAlO₃ perovskite with large surface area supported Ni-Based catalyst for methane dry reforming. *Catal. Lett.* **2022**, *152*, 2993–3003. [[CrossRef](#)]
16. Gangadharan, P.; Kanchi, K.C.; Lou, H.H. Evaluation of the economic and environmental impact of combining dry reforming with steam reforming of methane. *Chem. Eng. Res. Des.* **2012**, *90*, 1956–1968. [[CrossRef](#)]
17. Kawi, S.; Kathiraser, Y.; Ni, J.; Oemar, U.; Li, Z.; Saw, E.T. Progress in synthesis of highly active and stable nickel-based catalysts for carbon dioxide reforming of methane. *ChemSuschem* **2015**, *8*, 3556–3575. [[CrossRef](#)]
18. Abdulrasheed, A.; Jalil, A.A.; Gambo, Y.; Ibrahim, M.; Hambali, H.U.; Shahul Hamid, M.Y. A review on catalyst development for dry reforming of methane to syngas: Recent advances. *Renew. Sustain. Energy Rev.* **2019**, *108*, 175–193. [[CrossRef](#)]
19. Aramouni, N.A.K.; Touma, J.G.; Tarboush, B.A.; Zeaiter, J.; Ahmad, M.N. Catalyst design for dry reforming of methane: Analysis review. *Renew. Sustain. Energy Rev.* **2018**, *82*, 2570–2585. [[CrossRef](#)]
20. Bian, Z.; Das, S.; Wai, M.H.; Hongmanorom, P.; Kawi, S. A review on bimetallic Nickel-Based catalysts for CO₂ reforming of methane. *Chem. Phys. Chem.* **2017**, *18*, 3117–3134. [[CrossRef](#)]

21. Sharifianjazi, F.; Esmailkhanian, A.; Bazli, L.; Eskandarinezhad, S.; Khaksar, S.; Shafiee, P.; Yusuf, M.; Abdullah, B.; Salahshour, P.; Sadeghi, F. A review on recent advances in dry reforming of methane over Ni- and Co-based nanocatalysts. *Int. J. Hydrogen Energy* **2022**, *47*, 42213–42233. [[CrossRef](#)]
22. Baharudin, L.; Rahmat, N.; Othman, N.H.; Shah, N.; Syed-Hassan, S.S.A. Formation, control, and elimination of carbon on Ni-based catalyst during CO₂ and CH₄ conversion via dry reforming process: A review. *J. CO₂ Util.* **2022**, *61*, 102050. [[CrossRef](#)]
23. Pakhare, D.; Spivey, J. A review of dry (CO₂) reforming of methane over noble metal catalysts. *Chem. Soc. Rev.* **2014**, *43*, 7813–7837. [[CrossRef](#)] [[PubMed](#)]
24. Wang, S.; Lu, G.Q.M.; Millar, G.J. Carbon dioxide reforming of methane to produce synthesis gas over Metal-Supported catalysts: state of the art. *Energy Fuels* **1996**, *10*, 896–904. [[CrossRef](#)]
25. Nikoo, M.K.; Amin, N.A.S. Thermodynamic analysis of carbon dioxide reforming of methane in view of solid carbon formation. *Fuel Process Technol.* **2011**, *92*, 678–691. [[CrossRef](#)]
26. Li, Y.; Wang, Y.; Zhang, X.; Mi, Z. Thermodynamic analysis of autothermal steam and CO₂ reforming of methane. *Int. J. Hydrogen Energy* **2008**, *33*, 2507–2514. [[CrossRef](#)]
27. Shah, Y.T.; Gardner, T.H. Dry reforming of hydrocarbon feedstocks. *Catal. Rev.* **2014**, *56*, 476–536. [[CrossRef](#)]
28. Palmer, C.; Upham, D.C.; Smartm, S.; Gordon, M.J.; Metiu, H.; Mcfarland, E.W. Dry reforming of methane catalysed by molten metal alloys. *Nat. Catal.* **2020**, *3*, 83–89. [[CrossRef](#)]
29. Li, X.; Huang, Y. Study on the effect of reaction conditions on carbon deposition in dry reforming of methane. *Yunnan Chem. Technol.* **2021**, *48*, 18–21.
30. Anil, C.; Modak, J.M.; Madras, G. Syngas production via CO₂ reforming of methane over noble metal (Ru, Pt, and Pd) doped LaAlO₃ perovskite catalyst. *Mol. Catal.* **2020**, *484*, 110805. [[CrossRef](#)]
31. Wang, Y.; He, L.; Zhou, B.; Sheng, J.; Fan, J.; Li, W. Anti-coking NiCe/HAP catalyst with well-balanced carbon formation and gasification in methane dry reforming. *Fuel* **2022**, *329*, 125477. [[CrossRef](#)]
32. Sagar, V.T.; Pintar, A. Enhanced surface properties of CeO₂ by MnOx doping and their role in mechanism of methane dry reforming deduced by means of in-situ DRIFTS. *Appl. Catal. A* **2020**, *599*, 117603. [[CrossRef](#)]
33. Ramon, A.P.; Li, X.; Clark, A.H.; Safonova, O.V.; Marcos, F.C.; Assaf, E.M.; van Bokhoven, J.A.; Artiglia, L.; Assaf, J.M. In situ study of low-temperature dry reforming of methane over La₂Ce₂O₇ and LaNiO₃ mixed oxides. *Appl. Catal. B* **2022**, *315*, 121528. [[CrossRef](#)]
34. Wang, Q.; Wang, W.; Cao, M.; Li, S.; Wang, P.; He, J.; Li, R.; Yan, X. Effect of interstitial carbon atoms in core-shell Ni₃ZnCo_{0.7}/Al₂O₃ catalyst for high-performance dry reforming of methane. *Appl. Catal. B* **2022**, *317*, 121806. [[CrossRef](#)]
35. Yang, J.; Wang, J.; Zhao, J.; Bai, Y.; Du, H.; Wang, Q.; Jiang, B.; Li, H. CO₂ conversion via dry reforming of methane on a core-shell Ru@SiO₂ catalyst. *J. CO₂ Util.* **2022**, *57*, 101893. [[CrossRef](#)]
36. Ochoa, A.; Barbarias, I.; Artetxe, M.; Gayubo, A.G.; Olazar, M.; Bilbao, J.; Castaño, P. Deactivation dynamics of a Ni supported catalyst during the steam reforming of volatiles from waste polyethylene pyrolysis. *Appl. Catal. B* **2017**, *209*, 554–565. [[CrossRef](#)]
37. Fischer, F.; Tropsch, H. The preparation of synthetic oil mixtures (synthol) from carbon monoxide and hydrogen. *Brennst. Chem.* **1923**, *4*, 276–285.
38. Al-Fatesh, A.S.; Arafat, Y.; Kasim, S.O.; Ibrahim, A.A.; Abasaheed, A.E.; Fakeeha, A.H. In situ auto-gasification of coke deposits over a novel Ni-Ce/W-Zr catalyst by sequential generation of oxygen vacancies for remarkably stable syngas production via CO₂-reforming of methane. *Appl. Catal. B* **2021**, *280*, 119445. [[CrossRef](#)]
39. Wang, Y.; Zhang, R.; Yan, B. Ni/Ce_{0.9}Eu_{0.1}O_{1.95} with enhanced coke resistance for dry reforming of methane. *J. Catal.* **2022**, *407*, 77–89. [[CrossRef](#)]
40. Wang, D.; Littlewood, P.; Marks, T.J.; Stair, P.C.; Weitz, E. Coking can enhance product yields in the dry reforming of methane. *Acs Catal.* **2022**, *12*, 8352–8362. [[CrossRef](#)]
41. Wang, Z.; Cao, X.M.; Zhu, J.; Hu, P. Activity and coke formation of nickel and nickel carbide in dry reforming: A deactivation scheme from density functional theory. *J. Catal.* **2014**, *311*, 469–480. [[CrossRef](#)]
42. Donphai, W.; Faungnawakij, K.; Chareonpanich, M.; Limtrakul, J. Effect of Ni-CNTs/mesocellular silica composite catalysts on carbon dioxide reforming of methane. *Appl. Catal. A* **2014**, *475*, 16–26. [[CrossRef](#)]
43. Wang, N.; Xu, Z.; Deng, J.; Shen, K.; Yu, X.; Qian, W.; Chu, W.; Wei, F. One-pot synthesis of ordered mesoporous NiCeAl oxide catalysts and a study of their performance in methane dry reforming. *ChemCatChem* **2014**, *6*, 1470–1480. [[CrossRef](#)]
44. Sengodan, S.; Lan, R.; Humphreys, J.; Du, D.; Xu, W.; Wang, H.; Tao, S. Advances in reforming and partial oxidation of hydrocarbons for hydrogen production and fuel cell applications. *Renew. Sustain. Energy Rev.* **2018**, *82*, 761–780. [[CrossRef](#)]
45. Muraza, O.; Galadima, A. A review on coke management during dry reforming of methane. *Int. J. Energy Res.* **2015**, *39*, 1196–1216. [[CrossRef](#)]
46. Tsakoumis, N.E.; Rønning, M.; Borg, Ø.; Rytter, E.; Holmen, A. Deactivation of cobalt based Fischer-Tropsch catalysts: A review. *Catal. Today* **2010**, *154*, 162–182. [[CrossRef](#)]
47. Ranjekar, A.M.; Yadav, G.D. Dry reforming of methane for syngas production: A review and assessment of catalyst development and efficacy. *J. Indian Chem. Soc.* **2021**, *98*, 100002. [[CrossRef](#)]
48. Bartholomew, C.; Argyle, M. Advances in catalyst deactivation and regeneration. *Catalysts* **2015**, *5*, 949–954. [[CrossRef](#)]
49. Argyle, M.; Bartholomew, C. Heterogeneous catalyst deactivation and regeneration: A review. *Catalysts* **2015**, *5*, 145–269. [[CrossRef](#)]

50. Barrett, D.H.; Forbes, R.P.; Rodella, C.B. In situ and operando X-ray diffraction and X-ray absorption studies of Co-TiO₂ dry methane reforming catalysts. *J. Phys. D Appl. Phys.* **2020**, *53*, 44003. [[CrossRef](#)]
51. Zhang, X.; Deng, J.; Lan, T.; Shen, Y.; Qu, W.; Zhong, Q.; Zhang, D. Coking- and Sintering-Resistant Ni nanocatalysts confined by active BN edges for methane dry reforming. *ACS Appl. Mater. Interfaces* **2022**, *14*, 25439–25447. [[CrossRef](#)] [[PubMed](#)]
52. Chatla, A.; Almanassra, I.W.; Kallem, P.; Atieh, M.A.; Alawadhi, H.; Akula, V.; Banat, F. Dry (CO₂) reforming of methane over zirconium promoted Ni-MgO mixed oxide catalyst: Effect of Zr addition. *J. CO₂ Util.* **2022**, *62*, 102082. [[CrossRef](#)]
53. Liu, Y.; Chen, Y.; Gao, Z.; Zhang, X.; Zhang, L.; Wang, M.; Chen, B.; Diao, Y.; Li, Y.; Xiao, D.; et al. Embedding high loading and uniform Ni nanoparticles into silicalite-1 zeolite for dry reforming of methane. *Appl. Catal. B* **2022**, *307*, 121202. [[CrossRef](#)]
54. Han, B.; Wang, F.; Zhang, L.; Wang, Y.; Fan, W.; Xu, L.; Yu, H.; Li, Z. Syngas production from methane steam reforming and dry reforming reactions over sintering-resistant Ni@SiO₂ catalyst. *Res. Chem. Intermed.* **2020**, *46*, 1735–1748. [[CrossRef](#)]
55. Audasso, E.; Kim, Y.; Cha, J.; Cigolotti, V.; Jeong, H.; Jo, Y.S.; Kim, Y.; Choi, S.H.; Yoon, S.P.; Nam, S.W.; et al. In situ exsolution of Rh nanoparticles on a perovskite oxide surface: Efficient Rh catalysts for Dry reforming. *Korean J. Chem. Eng.* **2020**, *37*, 1401–1410. [[CrossRef](#)]
56. Cimino, S.; Lisi, L.; Mancino, G. Effect of phosphorous addition to Rh-supported catalysts for the dry reforming of methane. *Int. J. Hydrogen Energy* **2017**, *42*, 23587–23598. [[CrossRef](#)]
57. Chein, R.; Yang, Z.W. H₂S effect on dry reforming of biogas for syngas production. *Int. J. Energy Res.* **2019**, *43*, 3330–3345. [[CrossRef](#)]
58. Chein, R.; Chen, Y.; Chen, W. Experimental study on sulfur deactivation and regeneration of Ni-Based catalyst in dry reforming of biogas. *Catalysts* **2021**, *11*, 777. [[CrossRef](#)]
59. Misture, S.T.; Mcdevitt, K.M.; Glass, K.C.; Edwards, D.D.; Howe, J.Y.; Rector, K.D.; He, H.; Vogel, S.C. Sulfur-resistant and regenerable Ni/Co spinel-based catalysts for methane dry reforming. *Catal. Sci. Technol.* **2015**, *5*, 4565–4574. [[CrossRef](#)]
60. Gaillard, M.; Virginie, M.; Khodakov, A.Y. New molybdenum-based catalysts for dry reforming of methane in presence of sulfur: A promising way for biogas valorization. *Catal. Today* **2017**, *289*, 143–150. [[CrossRef](#)]
61. Nematollahi, B.; Rezaei, M.; Khajenoori, M. Combined dry reforming and partial oxidation of methane to synthesis gas on noble metal catalysts. *Int. J. Hydrogen Energy* **2011**, *36*, 2969–2978. [[CrossRef](#)]
62. Yentekakis, I.V.; Goula, G.; Hatzisymeon, M.; Betsi-Argyropoulou, I.; Botzolaki, G.; Kousi, K.; Kondarides, D.I.; Taylor, M.J.; Parlett, C.M.A.; Osatiashtiani, A.; et al. Effect of support oxygen storage capacity on the catalytic performance of Rh nanoparticles for CO₂ reforming of methane. *Appl. Catal. B* **2019**, *243*, 490–501. [[CrossRef](#)]
63. Jiménez, J.D.; Betancourt, L.E.; Danielis, M.; Zhang, H.; Zhang, F.; Orozco, I.; Xu, W.; Llorca, J.; Liu, P.; Trovarelli, A.; et al. Identification of highly selective surface pathways for methane dry reforming using mechanochemical synthesis of Pd-CeO₂. *ACS Catal.* **2022**, *12*, 12809–12822. [[CrossRef](#)] [[PubMed](#)]
64. Li, L.; Wu, S.; Li, H.; Deng, J.; Li, J. Preparation of novel mesoporous LaFeO₃-SBA-15-CTA support for syngas formation of dry reforming. *Nanomaterials* **2022**, *12*, 1451. [[CrossRef](#)] [[PubMed](#)]
65. Zambaldi, P.; Haug, L.; Penner, S.; Klötzer, B. Dry reforming of methane on NiCu and NiPd model systems: Optimization of carbon chemistry. *Catalysts* **2022**, *12*, 311. [[CrossRef](#)]
66. Sokefun, Y.O.; Trottier, J.; Yung, M.M.; Joseph, B.; Kuhn, J.N. Low temperature dry reforming of methane using Ru-Ni-Mg/ceria-zirconia catalysts: Effect of Ru loading and reduction temperature. *Appl. Catal. A* **2022**, *645*, 118842. [[CrossRef](#)]
67. Huang, Y.; Li, X.; Zhang, Q.; Vinokurov, V.A.; Huang, W. Enhanced carbon tolerance of hydrotalcite-derived Ni-Ir/Mg(Al)O catalysts in dry reforming of methane under elevated pressures. *Fuel Process. Technol.* **2022**, *237*, 107446. [[CrossRef](#)]
68. Liu, H.; Yu, J. Catalytic performance of Cu-Ni/La_{0.75}Sr_{0.25}Cr_{0.5}Mn_{0.5}O_{3-δ} for dry methane reforming. *Int. J. Energy Res.* **2022**, *46*, 10522–10534. [[CrossRef](#)]
69. Chaudhary, P.K.; Deo, G. Influence of particle size and metal-support interaction on the catalytic performance of Ni-Al₂O₃ catalysts for the dry and oxidative-dry reforming of methane. *Coll. Surf. A* **2022**, *646*, 128973. [[CrossRef](#)]
70. Sorcar, S.; Das, J.; Komarala, E.P.; Fadeev, L.; Rosen, B.A.; Gozin, M. Design of coke-free methane dry reforming catalysts by molecular tuning of nitrogen-rich combustion precursors. *Mater. Today Chem.* **2022**, *24*, 100765. [[CrossRef](#)]
71. Tang, Y.; Wei, Y.; Wang, Z.; Zhang, S.; Li, Y.; Nguyen, L.; Li, Y.; Zhou, Y.; Shen, W.; Tao, F.F.; et al. Synergy of Single-Atom Ni1 and Ru1 sites on CeO₂ for dry reforming of CH₄. *J. Am. Chem. Soc.* **2019**, *141*, 7283–7293. [[CrossRef](#)] [[PubMed](#)]
72. Akri, M.; El Kasmi, A.; Batiot-Dupeyrat, C.; Qiao, B. Highly active and Carbon-Resistant nickel Single-Atom catalysts for methane dry reforming. *Catalysts* **2020**, *10*, 630. [[CrossRef](#)]
73. Da Fonseca, R.O.; Rabelo-Neto, R.C.; Simões, R.C.C.; Mattos, L.V.; Noronha, F.B. Pt supported on doped CeO₂/Al₂O₃ as catalyst for dry reforming of methane. *Int. J. Hydrogen Energy* **2020**, *45*, 5182–5191. [[CrossRef](#)]
74. Jagódka, P.; Matus, K.; Sobota, M.; Bamacz, A. Dry reforming of methane over carbon Fibre-Supported CeZrO₂, Ni-CeZrO₂, Pt-CeZrO₂ and Pt-Ni-CeZrO₂ catalysts. *Catalysts* **2021**, *11*, 563. [[CrossRef](#)]
75. Al-Doghachi, F.A.J.; Islam, A.; Zainal, Z.; Saiman, M.I.; Embong, Z.; Taufiq-Yap, Y.H. High coke-resistance Pt/Mg_{1-x}Ni_xO catalyst for dry reforming of methane. *PLoS ONE* **2016**, *11*, e145862. [[CrossRef](#)] [[PubMed](#)]
76. Singha, R.K.; Shukla, A.; Sandupatla, A.; Deo, G.; Bal, R. Synthesis and catalytic activity of a Pd doped Ni-MgO catalyst for dry reforming of methane. *J. Mater. Chem. A* **2017**, *5*, 15688–15699. [[CrossRef](#)]
77. Dehimi, L.; Gaillard, M.; Virginie, M.; Erto, A.; Benguerba, Y. Investigation of dry reforming of methane over Mo-based catalysts. *Int. J. Hydrogen Energy* **2020**, *45*, 24657–24669. [[CrossRef](#)]

78. Liang, P.; Gao, H.; Yao, Z.; Jia, R.; Shi, Y.; Sun, Y.; Fan, Q.; Wang, H. Simple synthesis of ultrasmall β -Mo₂C and α -MoC_{1-x} nanoparticles and new insights into their catalytic mechanisms for dry reforming of methane. *Catal. Sci. Technol.* **2017**, *7*, 3312–3324. [CrossRef]
79. Shimura, K.; Fujitani, T. Effects of rhodium catalyst support and particle size on dry reforming of methane at moderate temperatures. *Mol. Catal.* **2021**, *509*, 111623. [CrossRef]
80. De Araújo Moreira, T.G.; de Carvalho Filho, J.F.S.; Carvalho, Y.; de Almeida, J.M.A.R.; Romano, P.N.; Sousa-Aguiar, E.F. Highly stable low noble metal content rhodium-based catalyst for the dry reforming of methane. *Fuel* **2021**, *287*, 119536. [CrossRef]
81. Khani, Y.; Shariatnia, Z.; Bahadoran, F. High catalytic activity and stability of ZnLaAlO₄ supported Ni, Pt and Ru nanocatalysts applied in the dry, steam and combined dry-steam reforming of methane. *Chem. Eng. J.* **2016**, *299*, 353–366. [CrossRef]
82. Wang, F.; Wang, Y.; Zhang, L.; Zhu, J.; Han, B.; Fan, W.; Xu, L.; Yu, H.; Cai, W.; Li, Z.; et al. Performance enhancement of methane dry reforming reaction for syngas production over Ir/Ce_{0.9}La_{0.1}O₂-nanorods catalysts. *Catal. Today* **2020**, *355*, 502–511. [CrossRef]
83. Wang, L.; Zhang, J.; Huang, J.; Cui, Q.; Zhu, Y.; Chen, H. Self-Confinement created for a uniform ir-Ni/SiO₂ catalyst with enhanced performances on CO₂ reforming of methane. *Energy Fuels* **2020**, *34*, 111–117. [CrossRef]
84. Chaudhary, P.K.; Koshta, N.; Deo, G. Effect of O₂ and temperature on the catalytic performance of Ni/Al₂O₃ and Ni/MgAl₂O₄ for the dry reforming of methane (DRM). *Int. J. Hydrogen Energy* **2020**, *45*, 4490–4500. [CrossRef]
85. Al Swai, B.M.; Osman, N.B.; Ramli, A.; Abdullah, B.; Farooqi, A.S.; Ayodele, B.V.; Patrick, D.O. Low-temperature catalytic conversion of greenhouse gases (CO₂ and CH₄) to syngas over ceria-magnesia mixed oxide supported nickel catalysts. *Int. J. Hydrogen Energy* **2021**, *46*, 24768–24780. [CrossRef]
86. Budiman, A.W.; Song, S.H.; Chang, T.S.; Choi, M.J. Preparation of a high performance cobalt catalyst for CO₂ reforming of methane. *Adv. Powder Technol.* **2016**, *27*, 584–590. [CrossRef]
87. Sukri, M.F.F.; Khavarian, M.; Mohamed, A.R. Effect of cobalt loading on suppression of carbon formation in carbon dioxide reforming of methane over Co/MgO catalyst. *Res. Chem. Intermed.* **2018**, *44*, 2585–2605. [CrossRef]
88. Han, J.W.; Park, J.S.; Choi, M.S.; Lee, H. Uncoupling the size and support effects of Ni catalysts for dry reforming of methane. *Appl. Catal. B* **2017**, *203*, 625–632. [CrossRef]
89. Budiman, A.W.; Song, S.; Chang, T.; Shin, C.; Choi, M. Dry reforming of methane over cobalt catalysts: A literature review of catalyst development. *Catal. Surv. Asia* **2012**, *16*, 183–197. [CrossRef]
90. Lin, X.; Zhang, Y.; Wang, Z.; Wang, R.; Zhou, J.; Cen, K. Hydrogen production by HI decomposition over nickel-ceria-zirconia catalysts via the sulfur-iodine thermochemical water-splitting cycle. *Energy Convers. Manag.* **2014**, *84*, 664–670. [CrossRef]
91. Jeon, O.S.; Lee, H.; Lee, K.; Paidi, V.K.; Ji, Y.; Kwon, O.C.; Kim, J.P.; Myung, J.; Park, S.Y.; Yoo, Y.J.; et al. Harnessing strong metal-support interaction to proliferate the dry reforming of methane performance by in situ reduction. *ACS Appl. Mater. Interfaces* **2022**, *14*, 12140–12148. [CrossRef]
92. Kwon, Y.; Eichler, J.E.; Mullins, C.B. NiAl₂O₄ as a beneficial precursor for Ni/Al₂O₃ catalysts for the dry reforming of methane. *J. CO₂ Util.* **2022**, *63*, 102112. [CrossRef]
93. Duan, X.; Pan, J.; Yang, X.; Wan, C.; Lin, X.; Li, D.; Jiang, L. Nickel-cobalt bimetallic catalysts prepared from hydrotalcite-like compounds for dry reforming of methane. *Int. J. Hydrogen Energy* **2022**, *47*, 24358–24373. [CrossRef]
94. Das, S.; Sengupta, M.; Patel, J.; Bordoloi, A. A study of the synergy between support surface properties and catalyst deactivation for CO₂ reforming over supported Ni nanoparticles. *Appl. Catal. A* **2017**, *545*, 113–126. [CrossRef]
95. Huang, C.; Zhang, Y.; Han, D.; He, B.; Sun, X.; Liu, M.; Mei, Y.; Zu, Y. Small-sized Ni nanoparticles embedded nickel phyllosilicate as a metal-acid bifunctional zeolite catalyst for cooperatively boosting CO₂-CH₄ reforming. *Fuel* **2023**, *331*, 125957. [CrossRef]
96. Jafarbegloo, M.; Tarlani, A.; Mesbah, A.W.; Sahebdehfar, S. One-pot synthesis of NiO-MgO nanocatalysts for CO₂ reforming of methane: The influence of active metal content on catalytic performance. *J. Nat. Gas Sci. Eng.* **2015**, *27*, 1165–1173. [CrossRef]
97. Ghodke, S.R.; Thundiyil, S.; Dongapure, P.; Nandini Devi, R. Effect of B site substitution in Gd₂B_{2-x}NiyO_{7-δ} (B = Ti, Zr) ternary metal oxide catalysts in dry reforming of methane. *Mol. Catal.* **2022**, *522*, 112242. [CrossRef]
98. Cao, A.N.T.; Pham, C.Q.; Nguyen, T.M.; Van Tran, T.; Phuong, P.T.T.; Vo, D.N. Dysprosium promotion on Co/Al₂O₃ catalysts towards enhanced hydrogen generation from methane dry reforming. *Fuel* **2022**, *324*, 124818. [CrossRef]
99. Sengupta, S.; Deo, G. Modifying alumina with CaO or MgO in supported Ni and Ni-Co catalysts and its effect on dry reforming of CH₄. *J. CO₂ Util.* **2015**, *10*, 67–77. [CrossRef]
100. Gerosa, M.; Bottani, C.E.; Caramella, L.; Onida, G.; Di Valentin, C.; Pacchioni, G. Defect calculations in semiconductors through a dielectric-dependent hybrid DFT functional: The case of oxygen vacancies in metal oxides. *J. Chem. Phys.* **2015**, *143*, 134702. [CrossRef]
101. Gambo, Y.; Jalil, A.A.; Triwahyono, S.; Abdulrasheed, A.A. Recent advances and future prospect in catalysts for oxidative coupling of methane to ethylene: A review. *J. Ind. Eng. Chem.* **2018**, *59*, 218–229. [CrossRef]
102. Djinović, P.; Batista, J.; Pintar, A. Efficient catalytic abatement of greenhouse gases: Methane reforming with CO₂ using a novel and thermally stable Rh-CeO₂ catalyst. *Int. J. Hydrogen Energy* **2012**, *37*, 2699–2707. [CrossRef]
103. Sophiana, I.C.; Iskandar, F.; Devianto, H.; Nishiyama, N.; Budhi, Y.W. Coke-Resistant Ni/CeZrO₂ catalysts for dry reforming of methane to produce Hydrogen-Rich syngas. *Nanomaterials* **2022**, *12*, 1556. [CrossRef] [PubMed]
104. Lanre, M.S.; Abasaheed, A.E.; Fakeeha, A.H.; Ibrahim, A.A.; Al-Awadi, A.S.; Jumah, A.B.; Al-Mubaddel, F.S.; Al-Fatesh, A.S. Lanthanum-Cerium-Modified nickel catalysts for dry reforming of methane. *Catalysts* **2022**, *12*, 715. [CrossRef]

105. Owgi, A.H.K.; Jalil, A.A.; Hussain, I.; Hambali, H.U.; Nabgan, W. Enhancing resistance of carbon deposition and reaction stability over nickel loaded fibrous silica-alumina (Ni/FSA) for dry reforming of methane. *Int. J. Hydrogen Energy* **2022**, *47*, 42250–42265. [[CrossRef](#)]
106. Zhu, R.; Ding, X.; Liu, Z.; Li, Y.; Wu, L.; Zheng, L.; Wang, Y. Promotional effects of Nd₂O₃ doped Ni/Al₂O₃-Y₂O₃ catalysts on oxygen vacancy and coking-resistant in dry reforming of methane. *Catal. Lett.* **2022**, *153*, 19–31. [[CrossRef](#)]
107. Wang, C.; Su, T.; Qin, Z.; Ji, H. Coke-resistant Ni-based bimetallic catalysts for the dry reforming of methane: Effects of indium on the Ni/Al₂O₃ catalyst. *Catal. Sci. Technol.* **2022**, *12*, 4826–4836. [[CrossRef](#)]
108. Liu, D.; Quek, X.; Wah, H.H.A.; Zeng, G.; Li, Y.; Yang, Y. Carbon dioxide reforming of methane over nickel-grafted SBA-15 and MCM-41 catalysts. *Catal. Today* **2009**, *148*, 243–250. [[CrossRef](#)]
109. Qian, L.; Ma, Z.; Ren, Y.; Shi, H.; Yue, B.; Feng, S.; Shen, J.; Xie, S. Investigation of La promotion mechanism on Ni/SBA-15 catalysts in CH₄ reforming with CO₂. *Fuel* **2014**, *122*, 47–53. [[CrossRef](#)]
110. Zhang, Q.; Zhang, T.; Shi, Y.; Zhao, B.; Wang, M.; Liu, Q.; Wang, J.; Long, K.; Duan, Y.; Ning, P. A sintering and carbon-resistant Ni-SBA-15 catalyst prepared by solid-state grinding method for dry reforming of methane. *J. CO₂ Util.* **2017**, *17*, 10–19. [[CrossRef](#)]
111. Kaydouh, M.N.; El Hassan, N.; Davidson, A.; Casale, S.; El Zakhem, H.; Massiani, P. Highly active and stable Ni/SBA-15 catalysts prepared by a “two solvents” method for dry reforming of methane. *Microporous Mesoporous Mater.* **2016**, *220*, 99–109. [[CrossRef](#)]
112. Zhu, L.; Lv, Z.; Huang, X.; Ran, J.; Chen, J.; Qin, C. Understanding the role of support structure in methane dry reforming for syngas production. *Fuel* **2022**, *327*, 125163. [[CrossRef](#)]
113. Moradi, G.; Khezeli, F.; Hemmati, H. Syngas production with dry reforming of methane over Ni/ZSM-5 catalysts. *J. Nat. Gas Sci. Eng.* **2016**, *33*, 657–665. [[CrossRef](#)]
114. Shiju, N.R. The role of metal-support bonding in controlling the particle size of Ceria-Supported transition metal catalysts. *ChemCatChem* **2011**, *3*, 112–114. [[CrossRef](#)]
115. González, J.J.; Da Costa-Serra, J.F.; Chica, A. Biogas dry reforming over Ni-Ce catalyst supported on nanofibred alumina. *Int. J. Hydrogen Energy* **2020**, *45*, 20568–20581. [[CrossRef](#)]
116. Peng, H.; Zhang, X.; Zhang, L.; Rao, C.; Lian, J.; Liu, W.; Ying, J.; Zhang, G.; Wang, Z.; Zhang, N.; et al. One-Pot facile fabrication of multiple nickel nanoparticles confined in microporous silica giving a Multiple-Cores@shell structure as a highly efficient catalyst for methane dry reforming. *ChemCatChem* **2017**, *9*, 127–136. [[CrossRef](#)]
117. Li, Z.; Mo, L.; Kathiraser, Y.; Kawi, S. Yolk-satellite-shell structured Ni-yolk@Ni@SiO₂ nanocomposite: Superb catalyst toward methane CO₂ reforming reaction. *ACS Catal.* **2014**, *4*, 1526–1536. [[CrossRef](#)]
118. Li, M.; Li, Z.; Lin, Q.; Cao, J.; Liu, F.; Wai, M.H.; Kawi, S. Sintering resistant cubic ceria yolk Ni phyllosilicate shell catalyst for methane dry reforming. *Catal. Today* **2022**, *402*, 319–327. [[CrossRef](#)]
119. Kim, S.; Lauterbach, J.; Sasmaz, E. Yolk-shell Pt-NiCe@SiO₂ Single-Atom-Alloy catalysts for low-temperature dry reforming of methane. *ACS Catal.* **2021**, *11*, 8247–8260. [[CrossRef](#)]
120. Wang, H.; Kim, S.; Sasmaz, E. Numerical investigation of the reaction kinetics of dry reforming of methane over the yolk-shell and single-atom alloy catalysts. *Chem. Eng. J.* **2022**, *450*, 138111. [[CrossRef](#)]
121. Kalai, D.Y.; Stangeland, K.; Li, H.; Yu, Z. The effect of La on the hydrotalcite derived Ni catalysts for dry reforming of methane. *Energy Procedia* **2017**, *142*, 3721–3726. [[CrossRef](#)]
122. Wang, J.; Zhang, G.; Li, G.; Liu, J.; Wang, Y.; Xu, Y.; Lyu, Y. Understanding structure-activity relationships of the highly active and stable La promoted Co/WC-AC catalyst for methane dry reforming. *Int. J. Hydrogen Energy* **2022**, *47*, 7823–7835. [[CrossRef](#)]
123. Seo, J.; Cho, E.; Kim, J.; Kim, S.B.; Youn, J.; Kim, D.H.; Ramasamy, P.K.; Lee, K.; Ko, C.H. Bifunctional metal doping engineering of Ni-supported alumina catalyst for dry methane reforming. *J. Environ. Chem. Eng.* **2022**, *10*, 108058. [[CrossRef](#)]
124. Nisa, K.S.; Suendo, V.; Sophiana, I.C.; Susanto, H.; Kusumaatmaja, A.; Nishiyama, N.; Budhi, Y.W. Effect of base promoter on activity of MCM-41-supported nickel catalyst for hydrogen production via dry reforming of methane. *Int. J. Hydrogen Energy* **2022**, *47*, 23201–23212. [[CrossRef](#)]
125. Zeng, F.; Zhang, J.; Xu, R.; Zhang, R.; Ge, J. Highly dispersed Ni/MgO-mSiO₂ catalysts with excellent activity and stability for dry reforming of methane. *Nano Res.* **2022**, *15*, 5004–5013. [[CrossRef](#)]
126. Tavasoli, A.; Ozin, G. Green syngas by solar dry reforming. *Joule* **2018**, *2*, 571–575. [[CrossRef](#)]
127. Zhou, L.; Martinez, J.M.P.; Finzel, J.; Zhang, C.; Swearer, D.F.; Tian, S.; Robotjazi, H.; Lou, M.; Dong, L.; Henderson, L.; et al. Light-driven methane dry reforming with single atomic site antenna-reactor plasmonic photocatalysts. *Nat. Energy* **2020**, *5*, 61–70. [[CrossRef](#)]
128. Du, Z.; Pan, F.; Yang, X.; Fang, L.; Gang, Y.; Fang, S.; Li, T.; Hu, Y.H.; Li, Y. Efficient photothermochemical dry reforming of methane over Ni supported on ZrO₂ with CeO₂ incorporation. *Catal. Today* **2022**, *409*, 31–41. [[CrossRef](#)]
129. Yang, Y.; Chai, Z.; Qin, X.; Zhang, Z.; Muhetaer, A.; Wang, C.; Huang, H.; Yang, C.; Ma, D.; Li, Q.; et al. Light-induced redox looping of a Rhodium/Ce_xWO₃ photocatalyst for highly active and robust dry reforming of methane. *Angew. Chem. Int. Ed.* **2022**, *61*, 202200567.
130. Zhang, Z.; Zhang, T.; Liang, W.; Bai, P.; Zheng, H.; Lei, Y.; Hu, Z.; Xie, T. Promoted solar-driven dry reforming of methane with Pt/mesoporous-TiO₂ photo-thermal synergistic catalyst: Performance and mechanism study. *Energy Convers. Manag.* **2022**, *258*, 115496. [[CrossRef](#)]
131. Gao, Y.; Li, Q.; Wang, C.; Yan, D.; Chen, J.; Jia, H. Light-driven efficient dry reforming of methane over Pt/La₂O₃ with long-term durability. *J. Mater. Chem. A* **2022**, *10*, 16016–16028. [[CrossRef](#)]

132. Snoeckx, R.; Zeng, Y.X.; Tu, X.; Bogaerts, A. Plasma-based dry reforming: Improving the conversion and energy efficiency in a dielectric barrier discharge. *RSC Adv.* **2015**, *5*, 29799–29808. [[CrossRef](#)]
133. Boulos, M.I.; Fauchais, P.; Pfender, E. *Handbook of Thermal Plasmas*; Springer: Berlin, Germany, 2016; pp. 1–34.
134. Snoeckx, R.; Bogaerts, A. Plasma technology—a novel solution for CO₂ conversion? *Chem. Soc. Rev.* **2017**, *46*, 5805–5863. [[CrossRef](#)] [[PubMed](#)]
135. Wang, Q.; Cheng, Y.; Jin, Y. Dry reforming of methane in an atmospheric pressure plasma fluidized bed with Ni/ γ -Al₂O₃ catalyst. *Catal. Today* **2009**, *148*, 275–282. [[CrossRef](#)]
136. Khoja, A.H.; Tahir, M.; Amin, N.A.S. Cold plasma dielectric barrier discharge reactor for dry reforming of methane over Ni/ γ -Al₂O₃-MgO nanocomposite. *Fuel Process. Technol.* **2018**, *178*, 166–179. [[CrossRef](#)]
137. Khoja, A.H.; Tahir, M.; Saidina Amin, N.A. Process optimization of DBD plasma dry reforming of methane over Ni/La₂O₃MgAl₂O₄ using multiple response surface methodology. *Int. J. Hydrogen Energy* **2019**, *44*, 11774–11787. [[CrossRef](#)]

Disclaimer/Publisher’s Note: The statements, opinions and data contained in all publications are solely those of the individual author(s) and contributor(s) and not of MDPI and/or the editor(s). MDPI and/or the editor(s) disclaim responsibility for any injury to people or property resulting from any ideas, methods, instructions or products referred to in the content.